AN ABSTRACT OF THE THESIS OF

William A. Siebold for the degree of Master of Science in Microbiology presented on April 2, 2001. Title: High-Resolution Digital Imaging of Bacterial Cells.

Abstract approved: Redacted for Privacy

Stephen J. Giovannoni

The most abundant clone found in ribosomal RNA clone libraries obtained from the world's oceans belongs to the SAR11 phylogenetic group of environmental marine bacteria. Imaging and counting SAR11 bacterial cells *in situ* has been an important research objective for the past decade. This objective has been especially challenging due to the extremely small size, and hypothetically, the low abundance of ribosomes contained by the cells. To facilitate the imaging of small dim oligotrophic bacterial cells, digital imaging technology featuring very small pixel size, high quantum yield scientific grade CCD chips was integrated with the use of multiple oligonucleotide probes on cells mounted on a non-fluorescing solid substrate.

Research into the composition of bacterioplankton populations in natural marine systems follows a two-fold path. Increasing the culturability of microbes found in the natural environment is one research path. Identifying and enumerating

the relative fractions of microorganisms *in situ* by culture-independent methods is another. The accumulation and systematic comparison of ribosomal RNA clones from the marine environment has resulted in a philosophical shift in marine microbiology away from dependence upon cultured strains and toward investigations of *in situ* molecular signals.

The design and use of oligonucleotide DNA probes targeting rRNA targets has matured along with the growth in size and complexity of the public sequence databases. Hybridizing a fluorescently labeled oligonucleotide probe to an rRNA target inside an intact cell provides both phylogenetic and morphological information (a technique called Fluorescence in situ Hybridization (FISH)). To facilitate the imaging of small, dim oligotrophic bacterial cells, digital imaging technology featuring very small pixel size, high quantum yield, scientific grade CCD chips is integrated with the use of multiple oligonucleotide probes on cells mounted on a non-fluorescing solid substrate.

This research develops the protocols necessary to acquire and analyze digital images of marine bacterial cells. Experiments were conducted with Bermuda Atlantic Time Series (BATS) environmental samples obtained during cruise BV21 (1998) and B138 (2000). The behavior of the SAR11[4]*Cy3 probe set when hybridized to bacterial cells from these samples was investigated to determine the optimal hybridization reaction conditions. The challenges of bacterial cell counting after cell transfer from PCTE membrane to treated microslides were addressed. Experiments with aged Oregon Coast seawater were performed to investigate the

protocol used to transfer cells from membrane to microslides, and examined the distribution of cells and the statistics of counting cells using traditional epifluorescence microscopy and image analysis techniques.

High Resolution Digital Imaging of Bacterial Cells

by

William A. Siebold

A THESIS

submitted to

Oregon State University

in partial fulfillment of
the requirements for the degree of

Master of Science

Presented April 2, 2001
Commencement June 2002

Master of Science thesis of William A. Siebold presented on April 2, 2001

APPROVED:

Redacted for Privacy

Major Professor, representing Microbiology

Redacted for Privacy

Chair of Department of Microbiology

Redacted for Privacy

Dean of Graduate School

I understand that my thesis will become part of the permanent collection of Oregon State University libraries. My signature below authorizes release of my thesis to any reader upon request.

Redacted for Privacy

William A. Siebold, author

TABLE OF CONTENTS

Page

INTRODUCTION..... 1

The Environment 1

Strategies 2

Digital Imaging and Fluorescence *in situ* Hybridization 5

Tools for Processing Digital Images 8

Fluorescence *in situ* Hybridization Experiments 16

METHODS 30

Sample collection and storage 30

Microslide preparation 32

Sample preparation 32

Fluorescence *in situ* hybridization and nuclear staining 36

Microscopy and image analysis 38

RESULTS AND DISCUSSION 41

BATS BV21 (1998) environmental cell analysis 41

BATS B138 (2000) environmental cell analysis 49

Oregon Coast environmental cell transfer analysis 53

TABLE OF CONTENTS (Continued)

CONCLUSIONS 75

Summary 75

Future work 75

BIBLIOGRAPHY 77

LIST OF FIGURES

Figure		Page
1.	Images and grey level histograms of clean microslide, black PCTE membrane and white PCTE membrane	6
2.	20 x 20 pixel region of the Digital Landscape	8
3.	Typical grey level histogram	11
4A.	Calculation of median filter in small neighborhood	12
4B.	Systematic application of filter across image	12
5.	Marr-Hildreth operator	13
6.	Segmentation by grey level thresholding	15
7.	Frequency of random occurrence of target sequence as a function of genome size	17
8.	Hybridization equilibrium conditions and oligonucleotide probe behavior	19
9.	Segmentation by Intensity Thresholding and Generation of the DAPI Mask	29
10.	BATS BV21 scatter plot of environmental surface sample object size and intensity characterization	43
11.	Image of BATS BV21 environmental surface sample	44
12.	BATS BV21 environmental surface sample wash temperature series	46
13.	BATS BV21 environmental surface sample bacterial and autofluorescent cells	47
14.	BATS B138 environmental Poisson distributions	52

LIST OF FIGURES (Continued)

15.	Microslide transfer evaluation Poisson distributions	56
16.	Artifacts presented by poor quality SuperFrost Plus microslides	59
17.	Images of SAR11 cells in transient culture	62
18.	Images of BATS BV21 environmental cell samples washed at 25°C.	65
19.	Images of BATS BV21 environmental cell samples washed at 32°C.	65
20.	Images of BATS BV21 environmental cell samples washed at 37°C and 42°C	66

LIST OF TABLES

Table		Page
1.	Oligonucleotide probes used in these experiments	36
2.	Mean object intensities from BATS BV21 environmental surface sample	42
3.	BATS environmental cell concentration protocol evaluation	49
4.	BATS B138 March 2000 Environmental Cell Counts	51
5.	Cell Counts for Microslide Transfer Protocol Evaluation	54
6.	Theoretical T_m and T_d for SAR11[4] Probe Set	63

HIGH RESOLUTION DIGITAL IMAGING OF MARINE BACTERIAL CELLS

INTRODUCTION

The Environment

The interface between the ocean surface and the atmosphere is an important boundary of active physical and chemical exchange. Elements and compounds shuttled across this border play an essential role in global biogeochemical cycles. An estimated thirty-three percent of the earth's photosynthesis occurs across this boundary. The dominant agents of photosynthetic activity in oligotrophic marine ecosystems are an extraordinarily diverse collection of aquatic photoautotrophs generally referred to as phytoplankton, which reside primarily in the surface layer of the world's oceans. In temperate oceans, the surface layer is characterized by significant gradients in light field, temperature and the concentration of reduced compounds of nitrogen. The key result of phytoplankton photosynthesis is the primary production of organic substrates from inorganic material. Photoautotrophs release biologically useful fixed carbon, by cell lysis, mechanical breakage by grazers, or active extracellular production from healthy (but leaky) cells (6). Approximately one-half of the fixed carbon so produced is directly utilized by heterotrophic bacterioplankton in a complex network of nutrient and energy resource partitioning among various biotic and abiotic aquatic compartments,

called the Microbial Loop (2). The past two decades have seen a dramatic reconsideration of the role of aquatic microbes in large biogeochemical cycles. Prokaryotes are currently considered the principal primary producers and heterotrophic consumers in marine ecosystems (3, 25, 27, 2, 7, 8).

The reevaluation of the importance of microbial activity in the world's oceans is a result of rapidly developing technologies in molecular biology in the early 1980's. For decades prior to this revolution in microbiological methods, inconsistencies had been observed between classical methods of enumerating cells from the ocean such as viable plate counts or most-probable number protocols, and direct microscopic cell counts. The bias represented by the classical techniques is obvious. The cell counts observed on plates are a function of the cells of the population that were able to grow on laboratory media whereas microscopy accounts for all cells, cultivable or not. In oligotrophic environments, direct cell counts by microscopy exceed viable-cell counts by several orders of magnitude, a phenomenon called the "great plate count anomaly" (24). The problem of why the vast majority of cells are currently uncultured remains an actively pursued research question.

Strategies

Research into the composition of bacterioplankton populations in natural marine systems follows two separate, but closely allied, paths. The effort to increase

culturability of microbes from natural environments is one path. The other path involves identifying and enumerating the relative fractions of microorganisms in the absence of culturing (culture-independent methods). Most traditional efforts toward understanding the role of microbial patches in the ocean have focused upon models that treat phyto- and bacterioplankton assemblages as "black boxes" through which elements and energy flux. Such studies have treated microbial processes as community averages, and have failed to address questions about the physiological activity of the individual participants. In the past two decades, the introduction of molecular methods has provided tools for cracking open the microbial black boxes, revealing bacterioplankton populations that are dominated by a relatively limited subset of phylogenetic groups that are widely distributed and may be variable in both spatial and temporal domains (22, 5). The cloning of ribosomal RNA genes from natural plankton communities provided the first insights into the biodiversity of marine microorganisms. The most abundant clone found in marine samples belongs to the SAR11 phylogenetic group. About 25% of all cells found in seawater belong to the SAR 11 group. Globally, the population size of SAR 11 is estimated to be greater than 10^{27}cells. SAR11 is an important microorganism in marine ecology. Typical ocean seawater contains up to two million microbial cells per cubic centimeter. Although these cells account for only 2% of all the microbial biomass on Earth, they are very active compared to most bacteria. About half of the photosynthesis, and the recycling of carbon, that occur

on the earth occur in the oceans, and SAR11, due to its abundance, is likely to play a significant role (9).

The accumulation and systematic comparison of ribosomal RNA clones from natural environments resulted in a philosophical shift in marine microbiology away from dependence upon cultured strains and toward investigations of *in situ* molecular signals. As the rRNA database grew in size and complexity, it became feasible to design oligonucleotide probes to specific bacterial groups. One method of applying oligonucleotide probes to environmental samples uses radioactively labeled probes hybridized to mixed genomic nucleic acids. The relative abundance of a specific 16S rRNA gene as a function of the total 16S rRNAs in the sample is calculated by dividing the amount of specific probe bound to a specific sample (in counts per minute) by the amount of hybridized universal probe. This method, called dot blot hybridization, has resulted in the discovery of novel new bacterial lineages (29), provided insights into the spatial relationships of marine microbes (5), and has furnished new information about the diversity of marine plankton (20, 21). Results gained from the use of this method must be evaluated in light of the varying ribosome content and rRNA operon copy number of bacterial cells. Most importantly, however, despite its utility, quantitative dot blot hybridization experiments fail to associate a given rRNA gene abundance with a specific cell morphology. Accurate cell counts and distributions of specific bacterial cells are therefore not possible.

Digital Imaging of Marine Bacteria and Fluorescence *in situ* Hybridization

Hybridizing a fluorescently labeled oligonucleotide probe to a ribosomal rRNA target inside an intact cell provides both phylogenetic and morphological information, a technique called Fluorescence in situ Hybridization (FISH). Using FISH methods, it is possible to visualize cell morphology, abundance, and distribution of uncultured microbes. The approach is challenging due to the small size and relatively low fluorescence signals obtainable from marine environmental cell samples.

To facilitate the imaging of the small dim cells associated with the SAR11 cluster of environmental gene clones, digital imaging technology featuring very small pixel size and high quantum efficiency scientific grade CCD chips is integrated with the use of multiple oligonucleotide probes (targeting a common phylogenetic group) on cells mounted on a non-fluorescing solid substrate. Dichromatic filter cubes are chosen to emphasize the isolation of the spectral bandwidths of interest.

The use of a scientific grade charge coupled device (CCD) at the intersection of the optical and digital-imaging components of the system is critical to the success of the application. Scientific grade CCD chips feature high sensitivity and quantum efficiency, excellent spatial resolution, low noise, high baseline stability, analytic linearity and sufficient dynamic and spectral ranges. Scientific

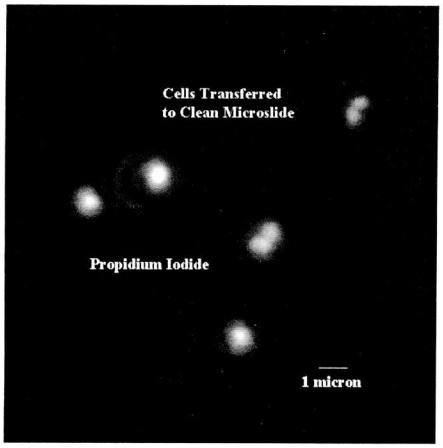

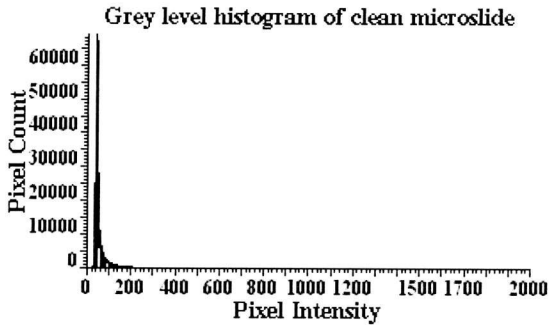

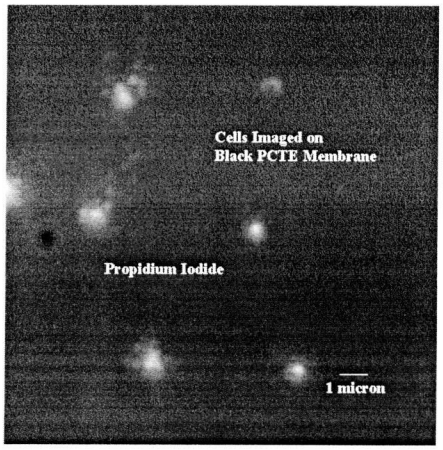

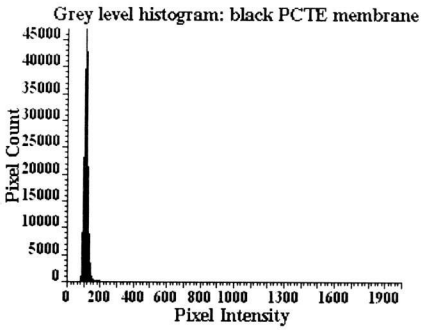

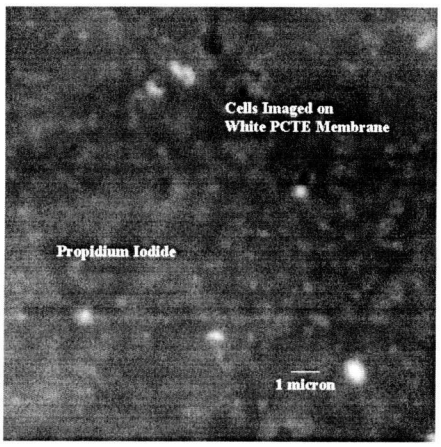

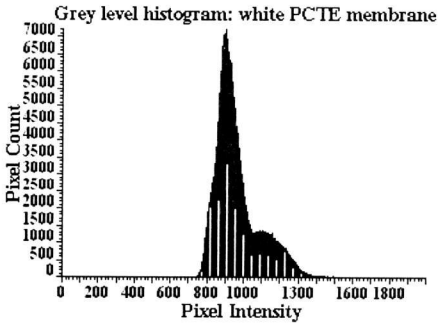

Figure 1.Images and grey level histograms of clean microslide, black PCTE membrane and white PCTE membrane. Note the elevated background and signal blurring for the membranes. The clean microslide displays a flat dark background grey level with good signal delineation. Propidium Iodide nuclear stain. 100X objective.

grade chips allow the collection of very low fluorescent signals using moderate integration times.

Performing hybridizations on polycarbonate (PCTE) membranes presents two problems that must be overcome. First, and more importantly, even the low background fluorescence of the membrane compromises the already tenuous signal to noise parameter when imaging small, dim cells (Figure 1). It is important, at all steps in the image acquisition and processing flow, to maximize the signal to noise ratio either by boosting signal (by the use of multiple probes) or by lowering background noise. A second problem presented by imaging cells on the membrane substrate involves slight, incrementally small deviations in the depth of field due to the slight unevenness of the membrane itself. The depth of field deviation was an issue across horizontal distances as low as twenty or thirty microns (i.e. within a single digital image frame). This second problem, while limiting in the present application, represents a fatal flaw in the more advanced cell array screening application, especially when Laser Scanning Cytometry is the instrumental method.

The use of high light throughput objectives, dichromatic mirrors and emission filters favors the acquisition of the maximum amount of fluorescence information while requiring only moderately long (1 –12 seconds) integration times. Objectives used should be corrected for spherical aberrations (deviations from perfect optical performance from the center of the field of view toward the edges) for the full spectral range (blue, green and red) of wavelengths. Objectives should also be corrected for chromatic aberrations in the blue, green and red

wavelengths. Dichromatic mirrors, excitation and emission filters are chosen for minimum spectral overlap between bandwidths.

The integrated use of scientific grade CCD detectors, image acquisition of objects mounted on a non-fluorescing solid substrate, and image filtering to extend the optical and digital properties of the acquisition system facilitates the imaging of very small, dimly fluorescing biological objects.

Tools for Processing Digital Images

The digital image can be considered as a landscape with topographical features (Figure 2). The topographical features may have the characteristics of tall, sharp mountain peaks, or of low, rolling hills, or both. The digital images most frequently encountered when acquiring epifluorescense images of environmental seawater samples tend to have similar attributes. The gray level histograms for the DAPI bandwidth, for example, tend to have a characteristic shape. The grey level histograms for probe bandwidths, however, are characteristically variable. Depending upon the bandwidth, the origin of the fluorescence emission, and the composition of cell types present in the image

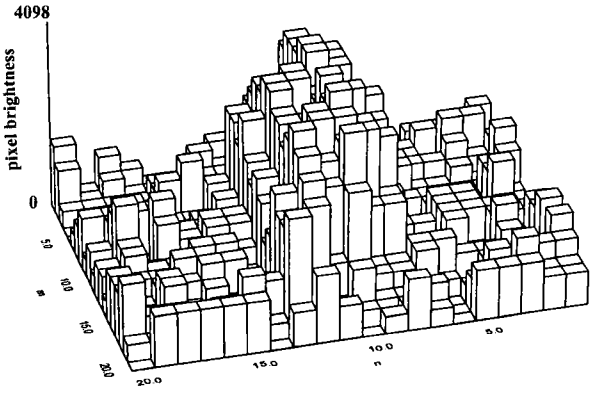

Figure 2. 20 x 20 pixel region of the Digital Landscape

being inspected, images may be relatively easy to manipulate or be impossible to reduce to useful information. It is critical to remember that the potential for any given digital image to be effectively analyzed is directly, and unavoidably, dependent upon the quality of the light source driving the optical components of the imaging system.

The fundamental goal of image analysis is to reduce a digital image to information. In the case of the present application, this refers to the ability to discriminate between digital objects (cells) and background, and to accurately define object boundaries such that it is possible to count and size them. The delineation of edges and boundaries is essential to this task. There are two levels of image analysis to be considered. First is semi-automated analysis of the image, where the analyst's eye is the primary discriminatory tool in the identification and delineation of objects of interest. The type of information required from the digital images encountered in the present application is especially accommodating to this method. In fact the human's eye and experience is more valuable and effective than the computer's objective criteria of object recognition (16). An experienced operator is capable of making 'run-time' decisions, distinguishing cellular objects from debris and other objects of ambiguous origin based upon pattern recognition with greater consistency than a computer. The computer is limited to a finite set of instructions based upon a limited number of inspection parameters. Semi-automated routines provide the analysis software with certain instructions which may drive the acquisition and storage of image frames, decide which object size

classes are to be included in an analysis, and electronically transfer digital masks from one image frame to another. The limitation to semi-automated analysis routines is the tedious nature of the work, more suited to development work than to production. These routines may be unavoidable when the signal to noise ratio, the general noise content of the images being processed, or the quality of the optical light source is unsatisfactory. The second level of image processing is the completely automated analysis of digital images, which includes all of the features described for semi-automated routines, but includes an additional pre-programmed set of criteria allowing the computer to identify and delineate objects of interest. Objects successfully identified by the recognition algorithm are then evaluated quantitatively. Data sets containing object counts and dimensional information are automatically formatted and sent to spreadsheet applications, where the information is arrayed and the objects are classified. Considering the variable nature of environmental samples and the variety of shapes, sizes, and intensities of objects of interest, the lack of a suitable pattern recognition algorithm is the single element that prevents reliable automated analysis protocols from becoming routine.

The effectiveness of both semi-automated and fully automated image analysis processing flows is dependent upon the quality of the digital image, which in turn is a product of optical image formation and the analog to digital conversion capabilities of the imaging system.

The gray level histogram is the fundamental diagnostic tool available when analyzing digital images. Gray level histograms are also known as brightness, or intensity histograms. Histograms count all of the pixels in a given region of interest that have a common intensity value and plot the relationships as peaks and valleys (Figure 3).

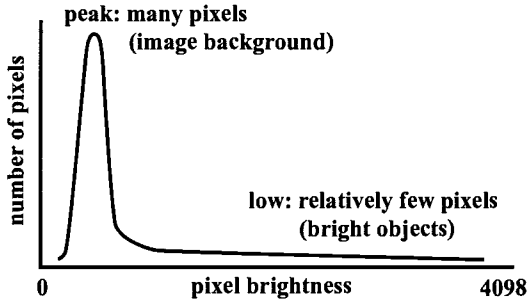

Figure 3. Typical grey level histogram

Peaks are relatively large numbers of pixels that have a common brightness value, or are contained within a narrow range of brightness values. The valleys, or lows, represent intensity values that are shared by relatively few pixels. Peaks are more common brightness values. Valleys are less common values. Calculation of the histogram involves loss of all positional information for all pixels. All of the pixels in a region of interest are included in the histogram. Twelve-bit data collected from a 1300 x 1030 pixel array requires that 1.3 million pixel brightness values be mapped onto a histogram confined to 4098 grey levels. The position, distribution, and delineation of histogram peaks is directly dependent upon the illumination source of the optical components, and is adversely affected by an inadequate signal to noise ratio, whatever the source.

Median filters, a category of rank value filters, are particularly useful early in the image processing flow. Median filters act in the spatial domain by

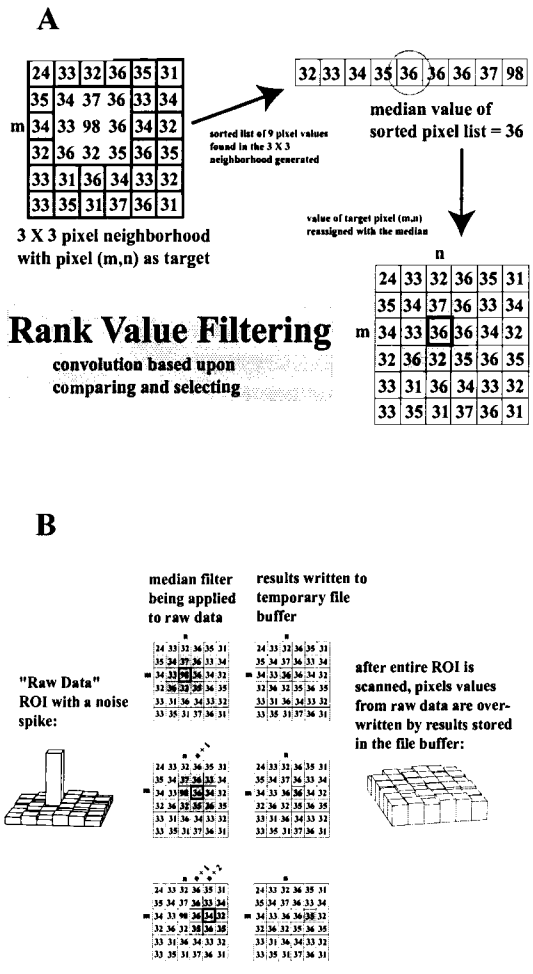

Figure 4. A: Calculation of median value in small neighborhood B: Systematic application of filter across image

systematically interrogating and storing pixel brightness values. Median operators rank the pixel intensity values in a small pixel neighborhood specified by the operator or programmer. Common neighborhoods are 3 x 3 or 5 x 5 squares of pixels (Figure 4). Median filters are useful for the rejection of random shot noise. Individual pixel brightness values may be corrupted, missing, or may be anomalously high relative to the entire pixel data array. Pixels with extreme brightness values (target pixels) are replaced with the median value for the target's surrounding neighborhood, resulting in a smoothing of the digital landscape. A critical benefit of median filtering in image processing flows is that brightness differences between objects and background are not compromised. Object boundaries are not shifted and only minimal edge degradation results. The median filter removes any inherent "roughness" of the digital landscape that may subsequently compromise the

effectiveness of downstream processing routines (including derivative operators and thresholding procedures).

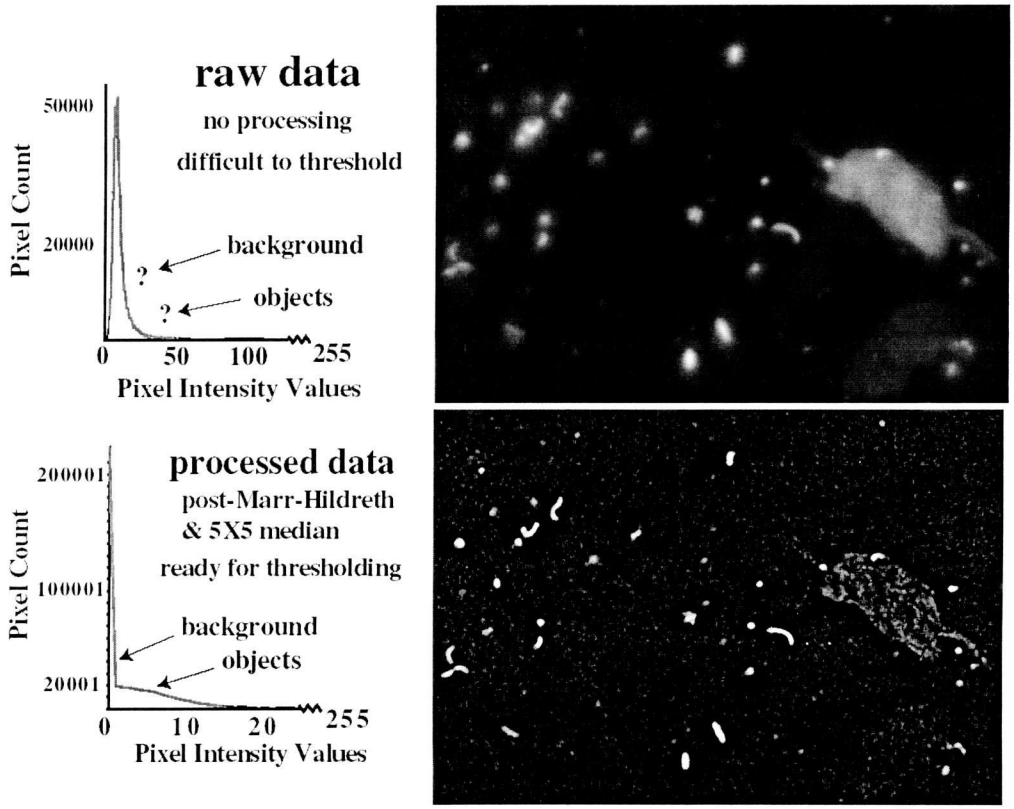

Figure 5. Marr-Hildreth operator. Comparison of digital images of environmental samples pre- and post-Marr-Hildreth derivative operator. Note the sharpness of the cell edges and elimination of the diffuse, obscuring noise in the latter image. The histograms to the left of the images illustrate the sharper discrimination of gray levels between object and background after edge definition. BATS B138 environmental surface cell sample. 100x objective

Derivative operators are primarily employed as a method of enhancing the edges of objects of interest. The operator used in the current experiments is a modified Marr-Hildreth second order derivative (R). This operator is most useful

when used on images obtained from environmental samples, whose objects of interest tend to be small with dense morphologies in the DAPI bandwidth. The modified Marr-Hildreth is less effective when applied to images obtained from cultured samples that include large objects of variable density, such as nuclear stained *Altermonas macleodii* cells. The primary benefit of using this operator on environmental images is the reduction of poorly defined artifacts and the tight, consistent segmentation criteria it provides for small, well-defined objects. The operator is usually applied to DAPI bandwidth image frames, which provide a sufficient background to object signal gradient for the operator to work upon (Figure 5).

Once an image has been pre-processed, segmentation by grey level thresholding is the technique most often used to reduce the image to useful information. Segmentation divides a region of interest into "object regions" based upon grey levels. Electronically defining features or objects on a digital image is a prerequisite to measurement and quantitative characterization. The analyst, or an algorithm written by the analyst, defines a range of brightness values, selects a set of pixels that fall within that range to keep, and rejects all others. It is an essential step in electronic boundary delineation.

Segmentation is an interactive process involving decisions based upon the grey level histogram. The result is a pixel-based representation of the image that assigns each pixel in the region of interest either to the classification of "object" or of "background". Pixels assigned to objects are passed on for further analysis.

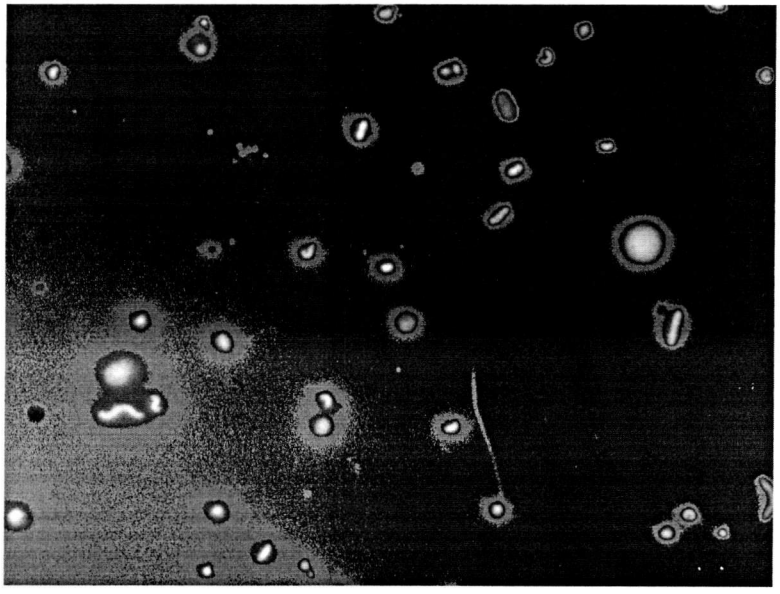

Figure 6. Segmentation by grey-level thresholding. Shaded regions represent a plane of identical grey level intensity values. The lower left portion of the image illustrates the problem of non-uniform illumination in the global thresholding of images acquired from marine environmental cell samples. BATS B138 environmental surface cell sample. 100X objective.

Problems with segmentation routines are the same as with most other processing steps. Inadequate signal to noise, erratic and uneven noise landscapes, ambiguous and poorly defined histogram peaks, uneven illumination, nonlinear camera response, analog to digital conversion errors, and optical focus errors may all act alone or in concert to prevent universal thresholding of a digital image frame (Figure 6).

Fluorescence *in situ* Hybridization Experiments

The determination of phylogenetic affiliation of marine bacterial cells by the design and application of ribosomal RNA-targeted oligonucleotide probes is fundamentally an exercise in balancing probe behavior under varying reaction conditions with the acquisition of analyzable signal. Oligonucleotide probes are short (ca. ten to fifty base-pairs long) single-stranded oligomers of DNA designed to have a nucleotide sequence complementary to a specific target ribosomal RNA sequence. An oligonucleotide probe's reaction behavior is governed by equilibrium conditions involving the hybridization reactions of the specific double helix formed when a probe collides with and binds to a complementary, or nearly complementary, sequence. A successful hybridization experiment results in 1). an optimal amount of oligonucleotide probe bound to the correct complementary target and 2). a signal that can be analyzed. These two conditions represent a balancing act between specific probe binding, non-specific probe binding and signal intensity.

An underlying assumption behind designing a probe to hit a phylogenetically specific target sequence is that the target sequence does not occur randomly but represents a phylogenetically distinct molecular signature. Equation 1 gives the frequency that a target sequence of length n will occur randomly in a DNA sequence of length L (23). The relationship between target length (and therefore probe length) and its frequency of random occurrence is illustrated in Figure 7 for genomes that are four million and one million base pairs long. The

$$f = (0.25)^n \times 2L$$

Equation 1. Frequency of random occurrence of target sequence of length n in DNA sequence of length L. Where f = frequency of occurrence, n = target length in nucleotides, L = length of double-stranded DNA sequence containing the random target

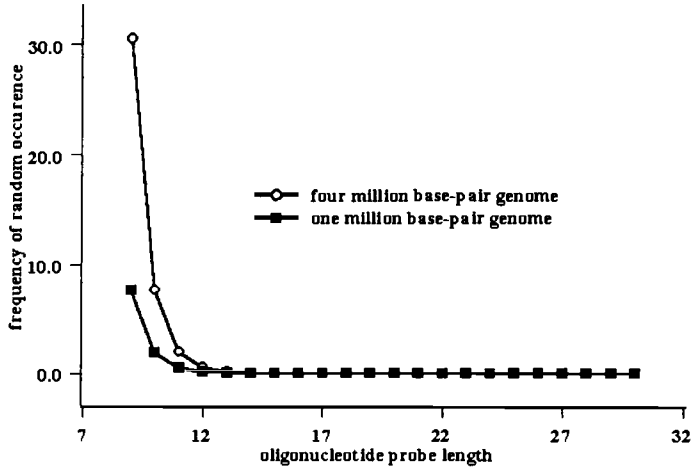

Figure 7. Frequency of random occurrence of target sequence as a function of genome size. Based on equation 1. Stahl & Amann, 1989.

frequency of an oligonucleotide probe eighteen nucleotides long colliding and binding to a randomly occurring complementary target sequence in a four million base pair genome is 1.2×10^{-4}. The very low probability of a given target sequence of useful length occurring randomly in a genome is a critical factor that makes the design and application of determinative oligonucleotide probes possible.

Stringency is a descriptive term identifying hybridization and wash factors governing the number of mismatches allowed in the hybrid probe:target duplex. *In situ* hybridization experiments are performed in two distinct steps, the hybridization phase and the wash phase. When applied to hybridization conditions stringency identifies the position of the reaction equilibrium with respect to the probe's ability or inability to bind promiscuously to sequences that are one, two or more base pair removed from exact target complementarity. Applied to the subsequent wash step stringency refers to the amount of mismatches that are allowed to remain in the duplex structure after washing. The stringency of the overall *in situ* hybridization reaction can be manipulated in either the hybridization or wash step.

Given an excess of probe relative to target the equilibrium conditions of the hybridization step are controlled by adjusting variables such as the ionic strength and formamide concentrations of the reaction reagents, the length and nucleotide composition of the probe and the temperature of the hybridization. Low stringency conditions allow more mismatches in the duplex product. High stringency conditions restrict the number of mismatches in the resulting hybrid duplex structure; the highest stringency allows no mismatches. If stringency conditions are severely limiting the probe may not bind to the desired target sequence with sufficient frequency. In this case the equilibrium has been shifted such that it does not favor probe binding to the desired exact complementary sequence. Generalized equilibrium conditions are illustrated in Figure 8.

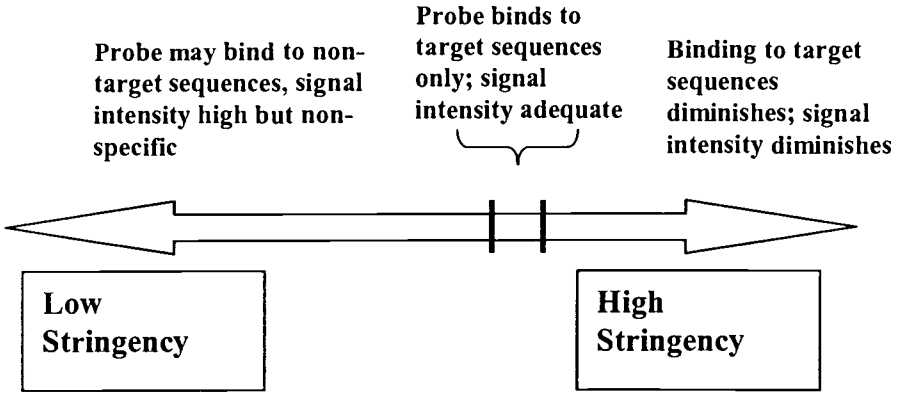

Figure 8. Hybridization equilibrium conditions and oligonucleotide probe behavior

Note that probe specificity and signal intensity are balanced over a relatively narrow range of conditions.

During the hybridization step the probe, in aqueous solution, is placed in close proximity to the target under reaction conditions favorable to DNA:RNA hybridization. The hybridization reaction follows first-order rate kinetics (26) and the extent of successful oligonucleotide binding is contingent upon the frequency of collisions between the probe and target. Hybridization reactions are dependent upon the concentration of the probe in the reaction mixture and an excess of probe is required to insure sufficient probe:target collisions (23). The relative influence of each of the reaction variables guiding probe specificity in the hybridization step is expressed in an empirically derived equation that calculates the theoretical melting temperature (T_m) of hybrid duplexes. For oligonucleotide probes between ten and fifty nucleotides long, Equation 2 accounts for the fraction of nucleotides in the

$$T_m = 81.5 + 16.6 \log M + 0.41[\%GC] - {}^{820}/_{n} - 0.7[\%\,formamide]$$

Equation 2. Calculation of theoretical melting temperature as a function of specificity factors for hybridization step. Where T_m= temperature of mid-point in transition from helix to random coil, M = molarity of monovalent cation [Na^+], %GC = guanine and cytosine content of probe, n= probe length in nucleotides. From Stahl & Amann, Development and Application of Nucleic Acid Probes, *in* Nucleic Acid Techniques in Bacterial Systematics, E. Stackebrandt and M. Goodfellow, ed. 1989.

probe that are guanine and cytosine (%GC), the molarity of monovalent ionic species (M), the concentration of formamide and the oligonucleotide probe length (n) (23). The complexity of the nucleotide sequence of the probe, expressed as the fraction of nucleotides that are guanine and cytosine, is a primary factor controlling the duplex melting temperature as long as the probe is present in significant excess of target. When all other factors are held constant in Equation 2, increasing the %GC of the probe by ten percent results in a 4.1°C increase in the melting temperature of a hybrid duplex (26). Using longer probes results in higher melting temperatures while enhancing specificity. However, the available target sequence length as observed in the sequence database may limit the probe length.

Once a probe has been designed, synthesized and applied to hybridization experiments, T_m may be manipulated by varying the monovalent cation concentration. Referring to Equation 2, there is a 16.6°C increase in T_m with each log increase in cation concentration. The use of organic solvents such as formamide that destabilize the helical structure of the hybrid duplex allows the experiment to

be performed at a lower temperature. Nucleic acids are degraded less and the reaction rates are greater when the experiment is performed at lower temperature (28,17). Adjusting formamide concentration to decrease the T_m facilitates greater probe specificity in the absence of elevated temperatures (17). In general, when performing multiple in situ hybridizations that require different stringency conditions it is easier to vary formamide concentrations and perform the hybridizations at a common temperature than it is to perform a series of hybridizations at varying temperatures.

The wash step of the hybridization reaction follows the hybridization step. Once the probe has been applied and has successfully bound to the target the resulting hybrid duplexes are washed to remove both excess unbound probes and non-specifically bound probe. The stringency of the overall reaction can be effectively determined during the wash step by careful consideration of the wash conditions. The wash buffer used to wash the hybrid duplexes differs from the hybridization buffer used in the probe-binding step. The molarity of the monovalent cation is lower and helix-destabilizing agents such as formamide are not present. A high-stringency wash may guarantee that only specifically bound probe is left for analysis or may result in removal of some or all of the specifically bound probe if stringency conditions are too severe. Equation 3 is an empirically derived equation describing the stringency and specificity criteria for the wash step (23, 26). It is similar to the equation for the hybridization step, but lacks a term for formamide concentration. In general, the same issue of probe specificity and signal intensity

$$T_d = 81.5 + 16.6 \log M + 0.41[\%GC] - {}^{820}/_{n}$$

Equation 3. Calculation of theoretical dissociation temperature (T_d) as a function of specificity factors for wash step. Where T_d= temperature of mid-point in transition of the dissociation of the hybrid duplex, M = molarity of monovalent cation [Na^+], %GC = guanine and cytosine content of probe, n= probe length in nucleotides. From Stahl & Amann, Development and Application of Nucleic Acid Probes, *in* Nucleic Acid Techniques in Bacterial Systematics, E. Stackebrandt and M. Goodfellow, ed. 1989.

must be considered when designing the wash step of the hybridization reaction. Washing at high stringency temperatures (or at low salt or high formamide concentrations) may remove specifically bound probe and reduce the resulting signal intensity.

Once a probe has been specifically bound to a target its activity must be detected and analyzed. Initial experiments using oligonucleotide probes in quantitative phylogenetic studies of marine microbes utilized radioactively labeled probes ([^{32}P]) hybridized to genomic DNA extracted from environmental samples and immobilized on a solid substrate. After hybridization and stringent washes the densitometric signal of the bound probe is collected and analyzed. This method has the benefit of quantitative sensitivity. The extraction of total nucleic acids from an environmental sample, however, results in the loss of all cell morphology information. The solid substrate-immobilized genome method yields information about the relative abundance of a specific gene sequence in a sample, but

disconnects that information from morphological information obtained by microscopic examination of cells. To simultaneously obtain both phylogenetic and morphological information, a technique that relies on microscopy is most useful. By attaching a single fluorescing molecular adjunct to one end of an oligonucleotide probe, specifically bound probe can be observed as a cellular signal using appropriate optical and digital hardware. To increase the fluorescent signal relative to background noise, multiple probes may be designed to target a common phylogenetic group. This has the effect of boosting the fluorescent signal for each cell.

In situ hybridizations can be performed on cultured cells or on environmental samples, where many of the cells are likely not to be available in culture. Ideally, *in situ* hybridizations are performed on cells with cultured representatives because the determination of experimental conditions and interpretation of analytical results is less ambiguous. The challenge of empirically determining the hybridization equilibrium and wash stringency conditions for a probe is very different when working with cultured versus environmental cells. The term *whole-cell* hybridization has been used in the literature (1) in a restrictive sense meaning hybridizations performed only on cultured cells. The term *in situ* hybridization will be used in a more general sense in this research to mean the hybridization of fluorescently labeled probes to either cultured or environmental bacterial cells.

In situ hybridization experiments on cells that have cultured representatives intrinsically include a positive control cell whose utility is to verify the effectiveness of the probe. Sequence analysis of a pure culture of cells provides an independent confirmation of the phylogenetic identity of the cells. Stringency may be controlled in the hybridization step of the reaction, where the T_m is the parameter of interest. When stringency conditions are controlled in the wash step of the reaction, the dissociation temperature (T_d) of the probe:target duplex is the parameter of interest. By hybridizing probes to cells under low stringency conditions and subsequently subjecting them to increasingly stringent wash conditions an empirical T_d may be obtained for that particular system of cells and probe. Experimental conditions that maximize the combination of probe signal and probe specificity can be determined with this information. It may be possible to obtain cultured cells whose sequence similarity to the target sequence of the cell of interest, whether it is cultured or uncultured, differs by one, two or more base mismatches. The determination of equilibrium conditions allowing or preventing probe binding to these cells further defines the limits of specificity of the probe to the intended target cell. Negative control probes, designed to have sequences coding for biological nonsense, can be applied to cultured cells and the background non-specific probe fluorescence signal intensity can be determined. Equilibrium or wash conditions may be modified to minimize the impact of this spurious background fluorescence on positive probe signals. The paramount question with respect to the success of the experiment is whether or not an observed positive

probe signal is caused by probe binding to the target sequence of interest. The possibility that the probe is binding non-specifically must be eliminated as an experimental concern. The causative relationship between positive fluorescence signal and specific probe binding can be established for cultured cells because it is possible to characterize the equilibrium and wash stringency system completely with the proper signal detection hardware.

The same is not true for *in situ* hybridization reactions performed on cells with no cultured representative. Because of the size and extent of public sequence databases, phylogenetically specific probes can be designed to target groups or members of groups of bacteria that have no cultured representative. Closing the causative loop between positive cell signals and specific probe binding under equilibrium and wash conditions is more difficult, and in some cases impossible, due to the lack of an intrinsic positive control cell. Without an independent identification by sequencing methods the question of whether or not the observed fluorescence signal is caused by probe binding to the intended complementary target sequence in the cell cannot be completely resolved. The best that may be accomplished is discovery of a cell morphology that consistently demonstrates a positive fluorescence signal when the probe is applied under defined reaction conditions. If distinct cell morphologies are observed consistently bound by probe to the exclusion of other morphologies, hybridization and wash conditions can be evaluated by probing identical environmental subsamples over a range of stringency conditions. Probe binding to characteristic cell morphology and not alternative

morphologies does not in itself prove the probe is binding as intended to the desired target sequence. If the observation remains consistent throughout a range of equilibrium and wash conditions it may be considered evidence supporting the hypothesis that the probe binding is due to a specific interaction with a complementary target sequence under defined reaction conditions.

Both cells and probes may provide controls for hybridization experiments. The primary purpose of hybridization controls is to establish that the cells of interest are binding probe because they contain the complementary target sequence and not because of random or non-specific binding.

The phylogenetic characterization of positive control cells, as previously described, is independently determined using molecular sequencing methods. Positive control cells provide information about cell morphologies whose target signature sequence is known. Negative control cells have signature sequences that differ from the target sequence of interest by one or more base-pair mismatches. Both positive and negative control cells provide valuable information with respect to reaction specificity. Sequence analysis and probe hybridizations of positive control cells are required to rigorously link positive fluorescence signals, specific probe binding and morphology.

Positive probes are designed to bind to a specific complementary target sequence. True positive probe signals result from the binding of a probe to cells that contain the correct complementary target sequence. The fluorescence intensity of positive signals is high relative to background or negative control probe intensities.

A positive probe may bind to cells that do not contain the correct complementary target sequence and exhibit high fluorescence signals relative to background. This non-specific binding is controlled in the analysis by using negative control probes on identical subsamples.

Negative control probes are designed by constructing sequences that code for biological nonsense. Reversing but not complementing a positive probe sequence will generate a nonsense sequence. In theory, negative control probes should not bind to the signature sequence of any cell. Prospective negative control probe sequences can be tested and verified by comparing the sequence against known sequences in the sequence databases. Negative control probe signals exhibit fluorescence intensities only slightly elevated from background when applied to any cell because they are designed specifically not to have a biologically sensible target. Relatively high fluorescence intensities may be observed if the negative control probe binds nonspecifically to cells. In environmental samples where autofluorescent cells confound the *in situ* analysis, negative control probes provide a method of distinguishing positive probe signals from autofluorescent signals. Total positive probe cell counts will include positive signals, non-specific signals and autofluorescent signals. Negative control probe cell counts will include non-specific signals and autofluorescent signals. Subtraction of the negative control probe cell counts from the total positive probe cell counts will yield the net number of cells in the sample bound by the positive probe. This method was used to analyze of BATS B138 environmental cell samples.

In FISH, fluorescence signals of varying intensities optically and digitally collected and supplied to the observer in the form of grey levels in digital image frames. The interpretation of fluorescence cell signals may be more complex that simply identifying bright positive probe signals and dim negative control probe signals. Positive probes may bind non-specifically to incorrect target sequences if the reaction conditions are not sufficiently stringent. This situation may not be obvious, especially when working with environmental samples, if cells with an expected morphology display bright signal. Alternatively, positive probe signals may be dim and approach background fluorescence values when the probe has been applied to cells whose morphology is consistent with that of the cell of interest. This underscores the importance of having an independent sequence identification of cell types linking morphology and target sequence. Given this information, all high intensity cell signals should correspond to the expected cell morphology (unless the bacterium of interest is pleomorphic) when hybridizing with the appropriate probe. However, not all cells of the expected morphology can be expected to demonstrate high intensity fluorescence signals under the same conditions. Phylogenetically different bacteria may share a common morphology, for example. This situation will be observed in the analysis of BATS B138 environmental cells.

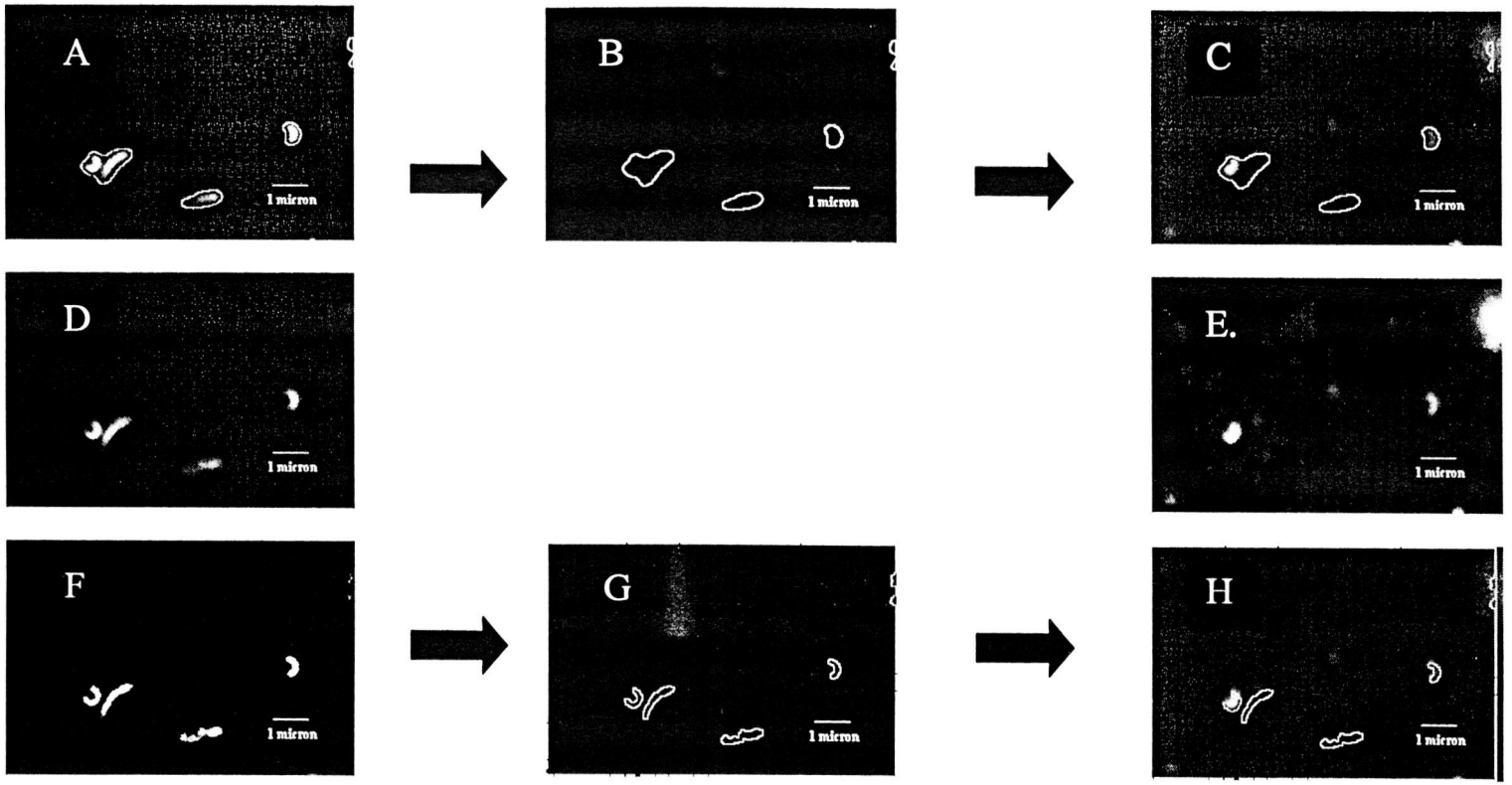

Figure 9. Segmentation by Intensity Thresholding and the Generation of the DAPI Mask. A.DAPI raw data with mask in place. B.raw data mask alone. C. raw data mask applied to SAR11[4]*Cy3 cells in 650/75-nm bandwidth. D. DAPI raw data. 100X objective. E. raw data from 650/75-nm (SAR11[4]*Cy3) bandwidth. F. DAPI image after application of Marr-Hildreth derivative operator. G. Marr-Hildreth mask. H. Marr-Hildreth mask applied to SAR11[4]*Cy3 cells in 650/75-nm bandwidth.

METHODS

Sample collection and storage

BATS cruise BV21 environmental cell samples

Cell Concentration Protocol: While on station at BATS in the Sargasso Sea on the R.V. Weatherbird II in April 1998, one measured liter of seawater was transferred from a Niskin bottle into an acid-washed polycarbonate carboy. The sample was immediately drawn down onto a 47 mm diameter 0.2 μm pore size, PCTE Nucleopore membrane through a polycarbonate inline filter module under gentle vacuum filtration (<7 p.s.i. Hg). During this process, caution was taken not to allow the membrane to go dry, to prevent the cells from sticking to the membrane. The filtration was stopped after the liter of sample was almost completely drawn through the inline filter module, allowing an air bubble to form around the filter module's inlet port. The inline filter module was detached from the vacuum lines and vortexed hard for one minute, dislodging the cells from the membrane and resuspending them. The vortexed sample, rich in cells, was removed from the filter module using a ten-milliliter sterile syringe attached to the inlet port. Approximately eight milliliters of sample was extracted from the module and transferred to a sterile fifteen milliliter Falcon tube. The cells were fixed in a 10% (v/v) solution of unbuffered formalin. formalin. Upon return to the Bermuda

Biological Station for Research (BBSR), a measured eight milliliter volume of the fixed cells were aliquoted into Oak Ridge tubes and centrifuged in a pre-chilled TI-880 rotor for one hour at 25,000 rpm. After centrifugation, the supernatant was carefully removed, without disturbing the pellet. One milliliter of a 50:50 (v/v) solution of 1X PBS (137 mM NaCl, 2.7 mM KCl, 4.3 mM $Na_2HPO_4 \bullet 7H_2O$, 1.4 mM KH_2PO_4, pH 7.3) and 100% EtOH was added and the tube vortexed for one minute to resuspend the cell pellet. The resuspended cells were transferred into a 1.5 milliliter cryogen tube, stored at -20°C, and subsequently shipped overnight to the lab at Oregon State University, Corvallis, OR in liquid nitrogen Dewars containers.

BATS cruise B138 environmental cell samples

Samples from 0, 20, 40, 80, 120, 160, 200 and 250 meters were taken from Niskin bottles on board R.V. Weatherbird II in March 2000 and immediately fixed in a solution of 10% (v/v) formalin and stored at 4°C. Fixed cell samples were filtered onto membranes after ca. eight hours and immediately transferred to microscope slides.

Oregon Coast environmental cell transfer experiment

Six samples were collected in six separate sterile fifteen-milliliter polyethylene screw cap tubes from a twenty-liter polycarbonate carboy containing

aged Oregon Coast seawater (two years at constant 15°C in twelve hour light/dark cycle), and fixed in a solution of 10% (v/v) tetraborate buffered formalin. The six samples were kept on ice until filtration and transfer onto microscope slides.

Microslide preparation

3-aminopropyltriethoxysilane (APES) microslide treatment: Inside a clean laminar flow hood, ultraclean (Fisher*finest*) microslides were placed in a glass Copeland jar containing 100% acetone for two minutes to remove oil, moisture, and loose debris. The microslides were transferred to a glass Copeland jar containing a 2% (v/v) solution of APES in acetone for two minutes. The microslides were then passed through two washes of nanopure water and placed in a clean metal container and covered with a lid. The container was baked in a vacuum micro-oven at 80°C under 30 in. Hg vacuum for fifteen minutes. After the slides were baked to dryness, the metal container was moved to the laminar flow hood and allowed to cool.

Sample Preparation

BATS cruise BV21 environmental cell samples

One hundred-microliter aliquots of concentrated cell suspension from stored cryogen tubes were transferred into one-milliliter of 1X PBS, vortexed gently for ten minutes to break up cell clusters and filtered down onto the shiny side of a

white standard 25 mm diameter, 0.2 μm pore size PCTE membrane using a 25 mm diameter, 0.8 μm pore size Metricell GN-4 membrane backing filter under gentle (< 7 p.s.i. Hg) vacuum pressure. The PCTE membrane and GN-4 backing filter were removed from the filter stack and placed cell side down onto a nanopure-rinsed SuperFrost Plus (VWR cat. # 48311-703) microscope slide. A second microscope slide was clamped on top of the membranes with binder clips, and the assembly was incubated at 42°C for one hour. After incubation, the slides were unclamped, and the PCTE and GN-4 membranes peeled off, leaving the cells adhered to the SuperFrost Plus microslide. The SuperFrost Plus slide was passed through an ethanol wash series (50, 80 and 100% EtOH, three minutes each) to dehydrate the cells. After dehydration, the SuperFrost Plus slide was allowed to dry, and stored at 4°C with desiccant.

BATS cruise B138 environmental samples

In Bermuda, ten-milliliters of fixed cell samples were filtered onto the shiny side of a 25 mm diameter, 0.2 μm pore size standard white PCTE membrane using a 25 mm diameter, 0.8 μm pore size Metricell GN-4 backing filter under gentle vacuum filtration (< 7 p.s.i. Hg). The PCTE and GN-4 membranes were removed from the filter stack and cut in half. Each half-membrane was placed cell side down on a SuperFrost Plus microslide. Microscope slides and binder clips were used to clamp the membranes in place, and the units were incubated at 42°C for one hour.

After incubation, the slides were unclamped, the membranes peeled off, and the microslides with the adhered cells were passed through an ethanol wash series (50, 80 and 100% EtOH, 3 minutes each), allowed to dry, and subsequently shipped overnight with desiccant to the lab at Oregon State University, Corvallis, OR. The slides were immediately stored at 4°C with desiccant at the OSU lab.

Oregon Coast environmental cell transfer experiment

Each of six polyethylene tubes containing fixed aged seawater cells was randomly chosen to deliver either seven or eleven-milliliter volumes of fixed cells to a clean filter stack. Three subsamples (two-eleven milliliter volumes and one-seven milliliter volume) were each filtered onto the shiny side of a 25 mm diameter, 0.2 μm pore size white standard PCTE membrane with a 25 mm diameter, 0.8 μm pore size Metricell GN-4 backing filter under gentle vacuum filtration (< 7 p.s.i. Hg). Immediately after each sample volume passed through the filter stack, the PCTE membrane and GN-4 backing filter were quickly transferred, cell side down, onto a 25 x 75-mm APES-coated ultraclean microslide (Fisher*finest* Premium cat. # 12-544-7) before the PCTE membrane could dry out. A four-inch rubber brayer was used to firmly press the membranes onto the treated microslide, insuring complete surface to surface contact. The pressed membrane was covered with a Metricell fiber support pad moistened with 20 μl of 0.02 μm filtered 1X PBS. The membrane and support pad were clamped into place on the treated microslide using a clean 25

x 75 mm plain use microslide and two small office binder clips. This assembly was incubated at 37°C for one hour. After incubation the clamped slides were separated and the membranes carefully peeled off, taking care not to disturb the cells now tightly bound to the treated microslide. The white standard PCTE membranes that were peeled off of the treated microslides were returned to the filter stack and covered with one-milliliter of 0.02 μm filtered 1X PBS containing 5 μg/ml 4,6-diamidinophenylindole dihydrate (DAPI, Molecular Probes, Eugene, OR) for ten minutes. The DAPI solution was filtered through the membrane and the membranes were removed from the filter stack and stored for later inspection. The three microslides were passed through an ethanol wash series (50, 80 and 100% EtOH, 3 minutes each), allowed to dry and stored in a dust and moisture free environment in the dark at 4°C. The other three subsamples (two-eleven milliliter volumes and one-seven milliliter volume) were each filtered onto the dull side of a 25 mm diameter, 0.2 μm pore size black PCTE membrane with a 25-mm diameter, 0.8 μm pore size, Metricell GN-4 backing filter, under gentle vacuum filtration (< 7 p.s.i. Hg). Prior to removal from the filter stack these membranes were covered with one-milliliter of 1X PBS containing 5 μg/ml DAPI for ten minutes. The DAPI solution was drawn through the membrane, which was then removed and mounted on a clean 25 x 75-mm plain use microscope slide with a (0.12-0.17 μm) coverslip (Polysciences cat. # 21913), and stored moisture free in the dark at 4°C.

Fluorescence in situ hybridization and nuclear staining

Oligonucleotide Probes

Oligonucleotide probes were stored as either 1-μg or 10-μg dried pellets, and brought to volume (working stock solution of 40 ng/μl) with the same hybridization solution used in the FISH experiments. Table 1 lists the probes used in these experiments.

Probe Name	Target Group	Sequence 5' to 3'
338R-FITC[a]	Bacteria	GCWGCCWCCCGTAGGWGT
EubA-FITC[a]	Bacteria	AAGGAGGTGATCCANCCVCA
27R-FITC[a]	Bacteria	CTGAGCCAKRATCRAACYCT
SAR11-541-Cy3[b]	SAR11	TCCGAACTACGCTAGGTC
SAR11-151-Cy3[b]	SAR11	ATTAGCACAAGTTTCCYCGTGT
SAR11-440-Cy3[b]	SAR11	TACAGTCATTTTCTTCCCCGAC
SAR11-731-Cy3[b]	SAR11	GTCAGTAATGATCCAGAAAGYTG
1521N-FITC[c]	Negative	ACGCCNACCTAGTGGAGGAA
338F-Cy3[c]	Negative	TGAGGATGCCCTCCGTCG

Table 1. Oligonucleotide probes used in these experiments.
a. set of three probes targeting bacteria: bac[3]*FITC
b. set of four probes targeting SAR11 group: SAR11[4]*Cy3
c. negative control probes: nonsense probes (reverse sequence of positive probe)
All probes designed by Stephanie Connon

BATS cruise BV21 and BATS cruise B138:

Twenty-microliters of hybridization solution (0.9M NaCl, 20mM Tris/HCl pH 7.4, 35% formamide, 0.01% SDS) (10) containing multiple oligonucleotide probes (Table 1), each at a final reaction concentration of 4 ng/μl, was placed in the center of the cell mass on the microslide. For each subsample of cells probed with either the bac[3]*FITC or the SAR11[4]*Cy3 suite of probes, an identical subsample was probed with negative control probes 1521N*FITC and 338F*Cy3. A standard 22 x 22-mm 0.22-mm coverslip (Fisherbrand cat. # 12-542B) was placed on the probe solution to facilitate even distribution of the probe solution across the cell mass and to prevent evaporation during incubation. The microslides were placed in a humid chamber containing hybridization solution and incubated for twelve hours at 32°C. After incubation, the microslides were transferred to the first of two Copeland jars containing pre-warmed (37°C) hybridization wash solution (70mM NaCl, 20mM Tris/HCl pH 7.4, 5mM EDTA, 0.01% SDS) (10). The coverslips were gently floated off the microslides with gentle agitation, and subsequently left in the wash solution for fifteen minutes. The microslides were then transferred to the second (37°C) hybridization wash solution for an additional fifteen minutes. BATS BV21 samples were also washed at a series of temperatures (25, 32, 37, 42 and 47°C) to establish wash stringency conditions. Following these washes, the

microslides were counterstained in a Copeland jar containing cold DAPI in hybridization wash solution (final concentration 5 μg/ml DAPI) for 10 minutes, and subsequently transferred to cold hybridization wash solution without DAPI for one minute. The slides were then allowed to dry. Coverslips (0.17 – 0.20 mm, Polysciences cat. # 21913) were mounted using Citifluor mountant media (Ted Pella cat. # 19470). The slides were stored with desiccant in the dark at 4°C.

Oregon Coast environmental cell transfer analysis:

Microslides with transferred cells were placed in a Copeland jar containing a solution of cold DAPI and hybridization wash (10) (final reaction concentration 5 μg/ml) for 15 minutes. The microslides were transferred to a cold hybridization wash without DAPI for one minute and subsequently allowed to dry. Coverslips (0.17 – 0.20 mm) were mounted using Citifluor as mountant. The microslides were stored dry, in the dark at 4°C.

Microscopy and Image Analysis:

Prepared slides were examined using a 100X (1.3 N.A., 0.17) Plan Fluotar infinity corrected (oil) objective mounted on a Leica DMRB microscope equipped with an epifluorescence module. The excitation light source was an Opti-Quip lamphouse with a 200 Watt Mercury burner. Dichromatic filter sets were as follows: UV/blue bandwidths (DAPI nuclear stain, absorption/emission maximums

ca. 358/461-nanometers) were collected with a 330WB80 excitation, 400DCLP01 dichromatic and 450DF65 emission filter set; green bandwidths (FITC and 6FAM fluorophores, absorption/emission maximums ca. 490/523-nanometers) were collected with a bp450/490 excitation, RKP510 dichromatic and sp580 emission filter set; orange/red bandwidths (Cy3 fluorophore, absorption/emission maximums ca. 554/568 nanometers and PI nuclear stain, absorption/emission maximums ca. 536/617 nanometers) were collected with a HQ545/30 excitation filter, Q565LP dichromatic, and HQ610/75 emission filter set. A standard C-mount and a 2X magnifier was used to mount a Princeton Instruments MicroMax 1300Y 5MZ cooled interline CCD camera (Meridian Instruments, Princeton, NJ). Nine-second (for DAPI) and twelve-second (for FITC, 6FAM and Cy3 fluorophores) integration times were used to collect 12-bit digital images (1300 x 1030 pixels, 4097 gray levels). Each digital image was a 1.34-million pixel array with scaled display dimensions of 39.2 X 31.06-μm using the 100X objective. One digital image frame per bandwidth (corresponding to DAPI, FITC/6FAM and Cy3) was collected per field of view, generating a total of three image frames per field of view. A minimum of ten fields of view were collected per sample. Digital images were processed using IPLab Spectrum version 3.2 image analysis software using semi-automated routines. Prior to analysis, images were routinely processed using a 3x3 median rank value digital filter to remove noise spikes and a histogram normalization routine to enhance signal and lower background for clear object delineation and, in some cases, to facilitate segmentation by thresholding. A

second order derivative linear shift-invariant operator (modified Marr-Hildreth operator, (22) followed by a 3x3 morphological opening operation, was occasionally used to subdue obscuring noise and to delineate sharp object edges, thereby facilitating object segmentation by gray level thresholding. A common protocol was to generate a 'boundaries only' segmentation mask on the image frame corresponding to the DAPI bandwidth. This mask was mapped onto image frames of the same field of view corresponding to the FITC and Cy3 bandwidths to locate and confirm positive or negative probe signals (Figure 9).

RESULTS AND DISCUSSION

BATS BV21 environmental cell analysis

Table 2 summarizes fluorescence data obtained by imaging cells from BATS BV21 environmental surface samples probed with the SAR11[4]*Cy3 probe set. The data suggest that signals can be assigned to one of four general types of objects. Positive signals in the 650/75-nm bandwidth had a mean fluorescence intensity of ca. 52 grey levels above background when probed with the SAR11[4]*Cy3 probe set. The objects showing positive signals possessed putative SAR11 morphology in the DAPI bandwidth based upon visual examination of SAR11 cells in culture (Connon et al, unpublished data) (Figure 17). DAPI stained objects having the SAR11 morphology displayed a low near-background signal (ca. 7 grey levels above background) in the 650/75-nm bandwidth when probed with the negative control probe 338F*Cy3. Autofluorescent cells emitted fluorescence signals in multiple bandwidths, were relatively large and were brighter than other objects (ca. 400 grey levels above background) (Figure 10). On digital image frames, they had elliptical, nearly circular shapes (Figure 13). A fourth group of objects, lumped together under the general term artifacts, is comprised of a wide variety of shapes, sizes and fluorescent intensities (mean intensity ca. 26.18 grey levels above background). Standard deviations (s) were large for each group. For positive SAR11[4]*Cy3 signals s = 25.02. For autofluorescent signals, s = 194.36.

	Fluorescence Signal			
	Positive Signal[a]	**Negative Signal[b]**	**Autofluorescent Signal[c]**	**Artifacts[d]**
Mean	51.97	7.02	399.87	26.18
Median	46.98	4.36	377.78	21.88
Standard deviation	25.02	7.94	194.36	27.57
Total objects	37	124	23	34

Table 2. Mean object intensities from BATS BV21 environmental surface sample. All values are reported as grey levels above local background. Hybridization with 35% formamide at 37°C. Washed at 37°C.

a. SAR11 morphologies reporting positive signal intensities in 650/75-nm bandwidth after probing with SAR11[4]*Cy3 probe set.
b. SAR11 morphologies as observed in 450/65-nm DAPI bandwidth, masked and transferred to 650/75-nm probe bandwidth. Probed with negative control probe 338F*Cy3.
c. Signal independent of positive or negative probe.
d. Diverse group of objects without definite cell-like structure. Sizes and shapes range from diffuse haze to pinpoint irregular particles.

Both negative control probe signals and artifacts had standard deviations in their brightness values nearly equal to the mean intensity (7.02, s = 7.94 and 26.18, s = 27.57, respectively). Figure 10 shows data from Table 2 plotted to visualize the relationships of the four major types of digital objects. Artifacts were diffuse and indistinct without well-defined edges or small, irregular shapes with mean area equal to 0.08 μm^2 (s = 0.06). Autofluorescent cells in this data set display areas ranging between ca. 0.1 and 0.5 μm^2 (mean = 0.22 μm^2, s = 0.09). Objects probed with the SAR11[4]*Cy3 probe set showing positive signals have a mean area equal to

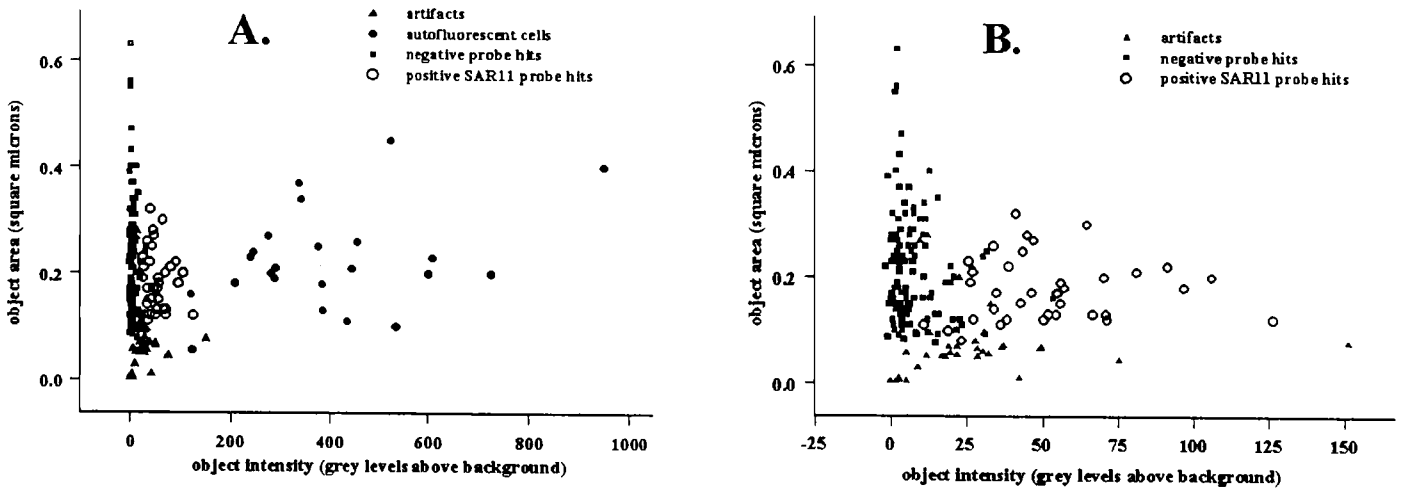

Figure 10. BATS BV21 environmental surface sample object characterization

A. Complete data set including positive SAR11[4]*Cy3 objects in 650/75-nm bandwidth, negative probe 338F*Cy3 objects (delineated by DAPI masking) in 650/75-nm bandwidth, autofluorescent cells and artifacts (non-cell objects).

B. Subset of data set A excluding autofluorescent cells illustrating relationships between positive SAR11 objects, negative control signal and artifacts.

0.18 μm^2 (s = 0.06, n = 37) and a median area equal to 0.17 μm^2. Objects identified in the DAPI bandwidth as having a putative SAR11 morphology and probed with the negative control probe 338F*Cy3 had a mean area equal to 0.21 μm^2 (s = 0.10, n = 124) and a median area equal to 0.18 μm^2.

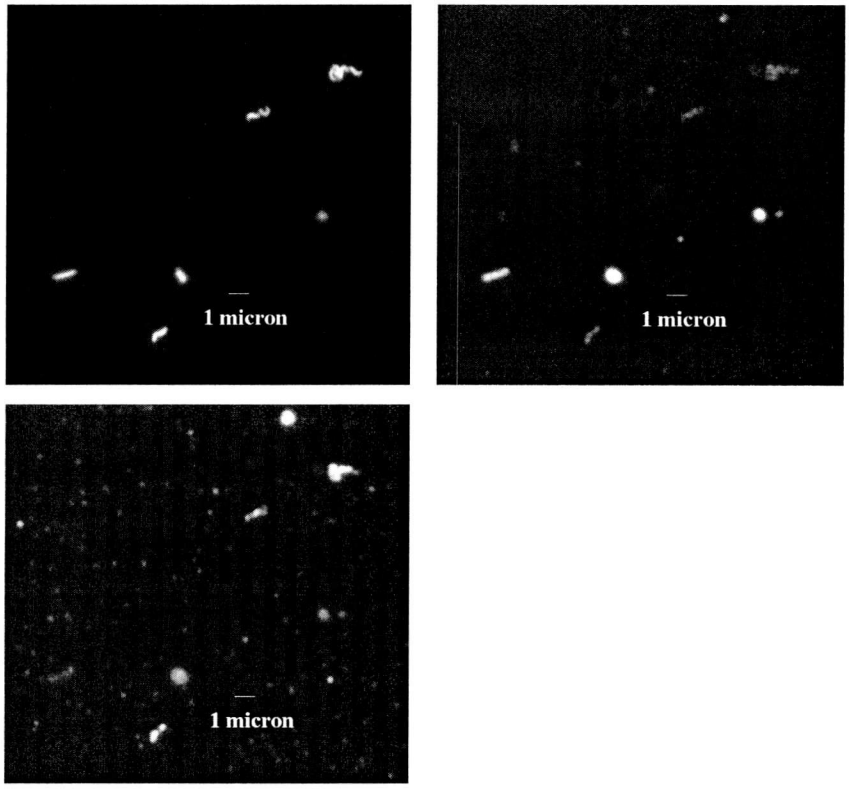

Figure 11. BATS BV21 environmental surface sample. Upper left: DAPI image. Upper right: bac[3]*FITC probe suite. Bottom left: SAR11[4]*Cy3 probe suite. Arrow points to cell yielding bright fluorescence signal relative to other cells in the bac[3]*FITC image and low level background fluorescence in SAR11[4]*Cy3 image. Hybridization at 32°C. Wash at 37°C. 100X objective

The series of digital images in Figure 11 (BATS BV21 environmental surface sample) illustrated the variability between positive and negative probe signals. The upper left image, taken with a three-second integration time in the 450/65-nanometer bandwidth, shows DAPI nuclear-stained environmental cells obtained from BATS surface in 1997. The image in the upper right, a twelve-second integration in the 510-580 nanometer bandwidth, is the same field of view showing bacterial cells probed with the bac^{3}*FITC probe set. Different cell types have different relative signal intensities. Two autofluorescent cells were large, round and bright in the higher probe bandwidths but are dim and difficult to see in the DAPI bandwidth. A single rod-shaped cell (see arrow in image) showed a strong signal when probed with the bac^{3}*FITC probe set, while other cells were not as bright but were positive signals nonetheless as indicated by a quantitative assessment of the average pixel intensity within the cell boundaries (data not shown). The lower left image, twelve-second integration in the 650/75-nanometer bandwidth, shows the cell signal resulting when the SAR11^{4}*Cy3 probe set is applied to the cells. The same rod-shaped cell showing a strong positive signal using the bac^{3}*FITC probe set shows a low-level negative background fluorescence signal using the SAR11^{4}*Cy3 set. Other putative SAR11 positive cell signals are relatively bright. This image illustrates the variability in signal intensity observed both between bandwidths and in the same bandwidth.

Relative signal intensities associated with putative SAR11 objects were plotted as a function of wash temperature in Figure 12. Fluorescence values plotted

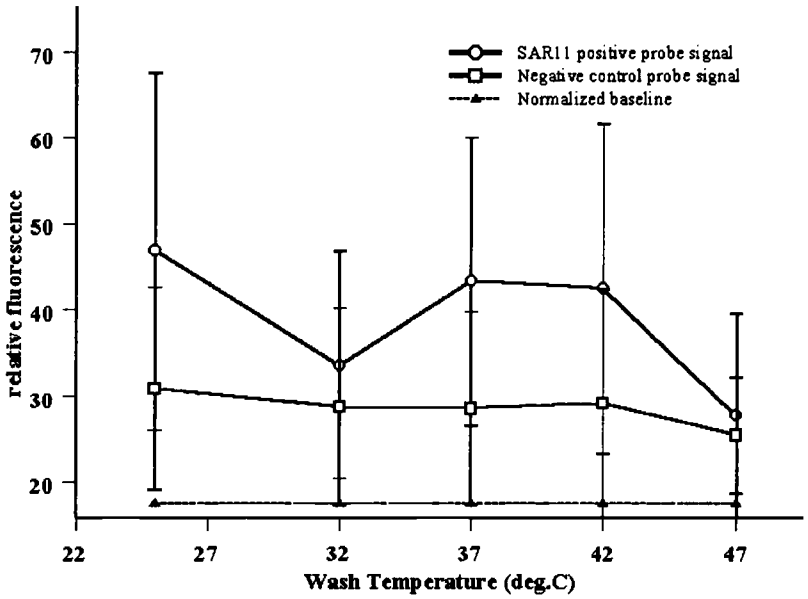

Figure 12. BATS BV21 environmental surface sample wash temperature series. Fluorescence values for positive probe (SAR11[4]*Cy3) and negative control probe (338F*Cy3) signals are normalized to common baseline fluorescence based upon mean background fluorescence values for ten microslides. Hybridizations at 32°C. Two fifteen-minute washes in 70mM Na^+ wash buffer at the indicated temperatures.

in Figure 12 were normalized to common baseline fluorescence for cells mounted on ten microslides. Positive signals obtained from cells mounted on five microslides probed with the SAR11[4]*Cy3 probe set showed an overall decline in magnitude with the highest values found at the lowest wash temperature. The standard deviation of intensity values for positive signals on the five microslides was large. The mean intensity of cell signals obtained washing at the lowest wash temperature (25°C) was 77.88 grey levels above background for nineteen objects (s = 34.45). At the highest wash temperature used in the evaluation, 47°C, mean cell

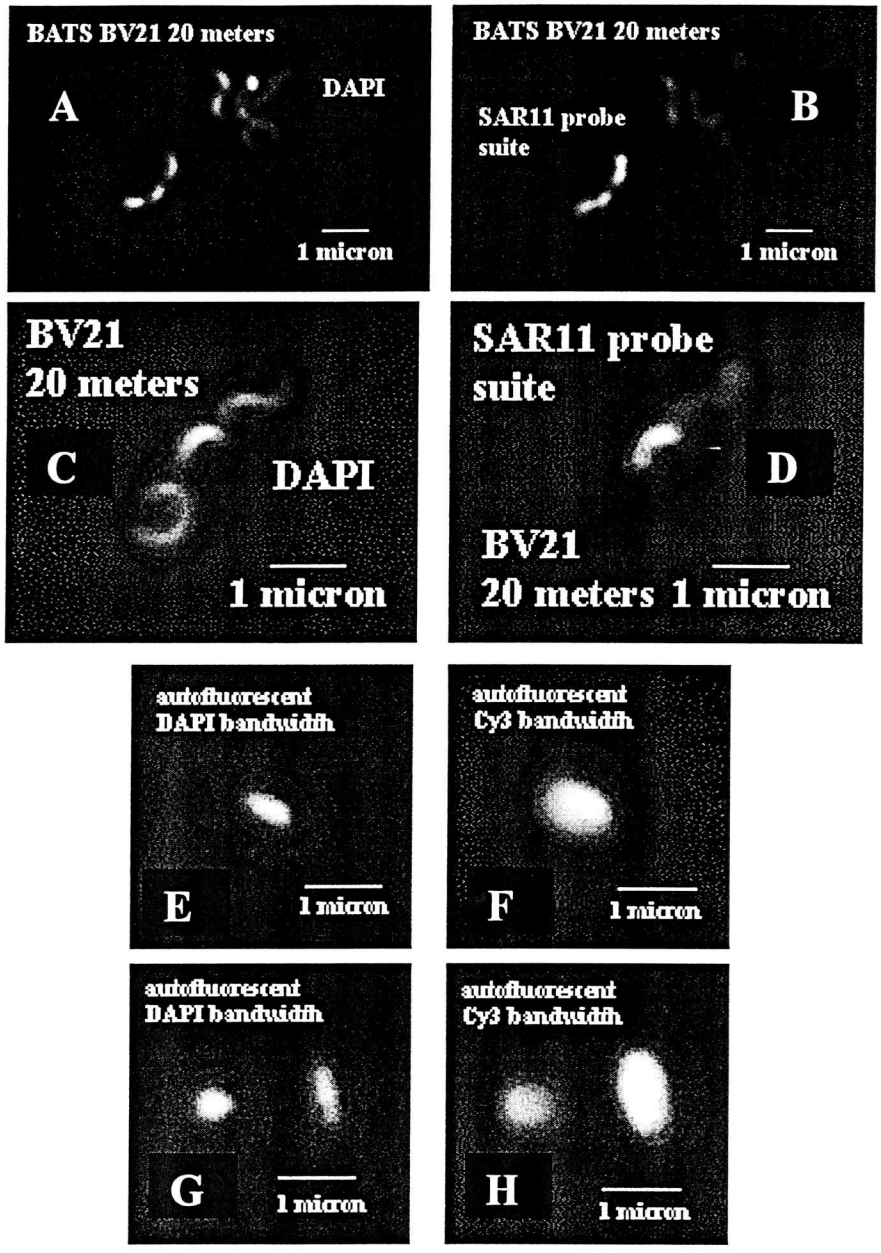

Figure 13. BATS BV21 environmental surface sample bacterial and autofluorescent cells.

A. DAPI stained cells with SAR11 morphology
B. same field of view as A; cells probed with SAR11[4]*Cy3
C. DAPI stained cells with SAR11 morphology
D. same field of view as C; cells probed with SAR11[4]*Cy3

E and G: Autofluorescent cells in 450/65-nm bandwidth
F and H: Autofluorescent cells in 650/75-nm bandwidth
Hybridization at 32 C. Wash at 37 C. 100X objective

intensity was 36.55 grey levels above background for twenty-three objects (s = 15.67). At 32°C wash temperature the mean cell signal was 49.39 grey levels above background (s = 19.34) for 20 objects. At 37 and 42°C the positive probe signal was 65.28 (s = 25.14) and 59.50 (s = 26.83) grey levels above background for 23 and 29 objects, respectively. Measurements of the fluorescence background of the five microslides probed with SAR11[4]*Cy3 and washed at 25, 32, 37, 42 and 47°C were very close at 29.07 (s = 4.53), 25.70 (s = 2.33), 26.34 (s = 3.96), 24.49 (s = 1.71) and 23.03 (s = 1.33). Mean cell intensities for cells with putative SAR11 morphology (imaged and masked using the DAPI bandwidth) and probed with negative control probe 338F*Cy3 were low. At 25°C the negative probe signals averaged 6.00 grey levels above background (s = 6.01). At 32°C the negative probe signals averaged 5.93 grey levels above background (s = 6.05). At 37 and 42°C the mean negative probe cell intensity was 5.85 (s = 5.91) and 6.17 (s = 6.98). At 47°C the mean negative probe intensity was 6.10 (s = 7.25). Background intensities between the five microslides probed with negative control probe 338F*Cy3 were consistent (15.21, 15.14, 15.06, 15.38 and 15.30).

Cell counts of concentrated BATS BV21 environmental samples after one year of storage in 50:50 1XPBS/EtOH at the laboratory at Oregon State University (OSU) revealed significantly low cell retention rates when compared to direct cell counts on samples not subjected to the concentration protocol (Table 3). Quality control testing during development of the cell concentration protocol initially disclosed cell retention rates approaching 70 to 80% (Brian Lanoil, personnel

BATS Sample #	Concentrated Sample[a.] DAPI Counts (cells/ml x 10^7)	BATS[b.] Direct Counts (cells/ml x 10^8)	Percent of Cells Recovered from Cell Concentration Protocol
BV21-1	2.34	5.96	2.80%
B114-1	0.851	3.56	2.39%
B110-1	0.294	4.84	0.61%
B113-1	1.18	4.55	2.59%
BV21-5	1.84	6.01	1.93%
BV21-6	1.93	2.67	7.23%

Table 3. BATS environmental cell concentration protocol evaluation
a. DAPI counts of concentrated cells stored in 50:50 1XPBS/EtOH at OSU laboratory. Counts performed one-year after concentration and storage
b. Direct cell counts of original environmental sample prior to concentration protocol. Performed by BATS personnel

comm.). The discovery of low retention rates one-year later was supported by independent tests performed by BATS personnel (data not shown).

BATS B138 environmental cell counts

Examination of six sample microslides verified that the cell transfer efficiencies for this experiment were low for all samples (Table 4.). Transfer efficiencies for samples obtained from zero and forty-meter depths were all between fifty and ninety-percent. The percent of cells transferred to the twenty-meter slides was 32.26 and 22.75% for the positive probe and negative control probe slides, respectively. The highest transfer efficiency observed in the data set was 88.43% (forty-meter negative control slide). The average number of cells

detected per image frame for the zero-meter positive probe slide was 24.5 (s = 9.13) and is 15.1 (s = 6.44) for the corresponding negative control probe slide. The twenty-meter positive probe slide had 10.7 cells per image frame (s = 4.93) compared to 7.5 (s = 4.91) for the negative control probe slide for the same depth. The average number of cells observed per image frame on the forty-meter positive probe slide was 25.6 (s = 9.56). The forty-meter negative control probe slide had 32.3 cells per image frame (s = 12.22). The variation in cell numbers detected per image frame between identical subsamples implies that the observed discrepancies are due to the transfer protocol.

Construction of six sample distributions and application of the Chi-square Goodness-of-Fit test indicated that there was insufficient evidence to reject the null hypothesis (H_0) that the cells are distributed in a Poisson manner for five of the six microslides analyzed (Figure 14). H_0 was rejected in the case of the twenty-meter positive probe slide. The magnitude of the calculated Chi-square test statistic varied between the six distributions. The zero-meter positive probe slide distribution and the twenty-meter negative control probe slide distribution had the low values at 8.11 and 7.56, respectively. Calculated test statistics for other distributions were 12.38, 22.36 and 20.37. The twenty-meter positive probe slide distribution had a chi-square test statistic of 34.99, greater than the tabulated threshold of 22.36 set at thirteen degrees of freedom at the 0.05 level of significance (Figure 14.).

Cell Abundance X 10^5 cells/ml						
Depth	BATS[a] Direct Counts	Transfer Microslide				SAR11 (% Direct)[g]
		DAPI (450/65-nm)[e]		Cy3 (650/75-nm)[f]		
		Positive[b] (transfer %)[c]	Control[d] (transfer %)[c]	Positive[b]	Control[d]	
0 m	6.68	5.47 (81.93)	3.37 (50.49)	3.35	2.57	0.79 (11.79%)
20 m	7.41	2.39 (32.26)	1.69 (22.75)	3.87	2.10	1.76 (23.81%)
40 m	8.25	5.79 (70.19)	7.30 (88.43)	3.76	1.02	2.73 (33.14%)

Table 4. BATS B138 March 2000 Environmental Cell Counts.

a. Direct cell counts by BATS personnel in Bermuda. Slide prepared 3/16/00. Cell counts on black PCTE membrane independent of transfer protocol
b. Positive transfer slide probed with SAR11[4]*Cy3 probe suite and DAPI counterstained
c. Calculated as percentage of cell counts on transfer microslide relative to BATS direct counts (a.)
d. Negative control transfer microslide probed with 338F*Cy3 and DAPI counterstained
e. Fluorescence bandwidth sampled for DAPI counterstain. Cell counts on transfer microslide.
f. Fluorescence bandwidth sampled for SAR11[4]*Cy3 and 338F*Cy3 probe signal. Cell counts in the Cy3 bandwidth have been corrected for cell transfer % (c.)
g. Calculated as difference between corrected positive transfer microslide SAR11 cell counts and corrected negative control microslide SAR11 cell counts. Ratio of the resulting values with BATS Direct Counts is reported in parentheses.

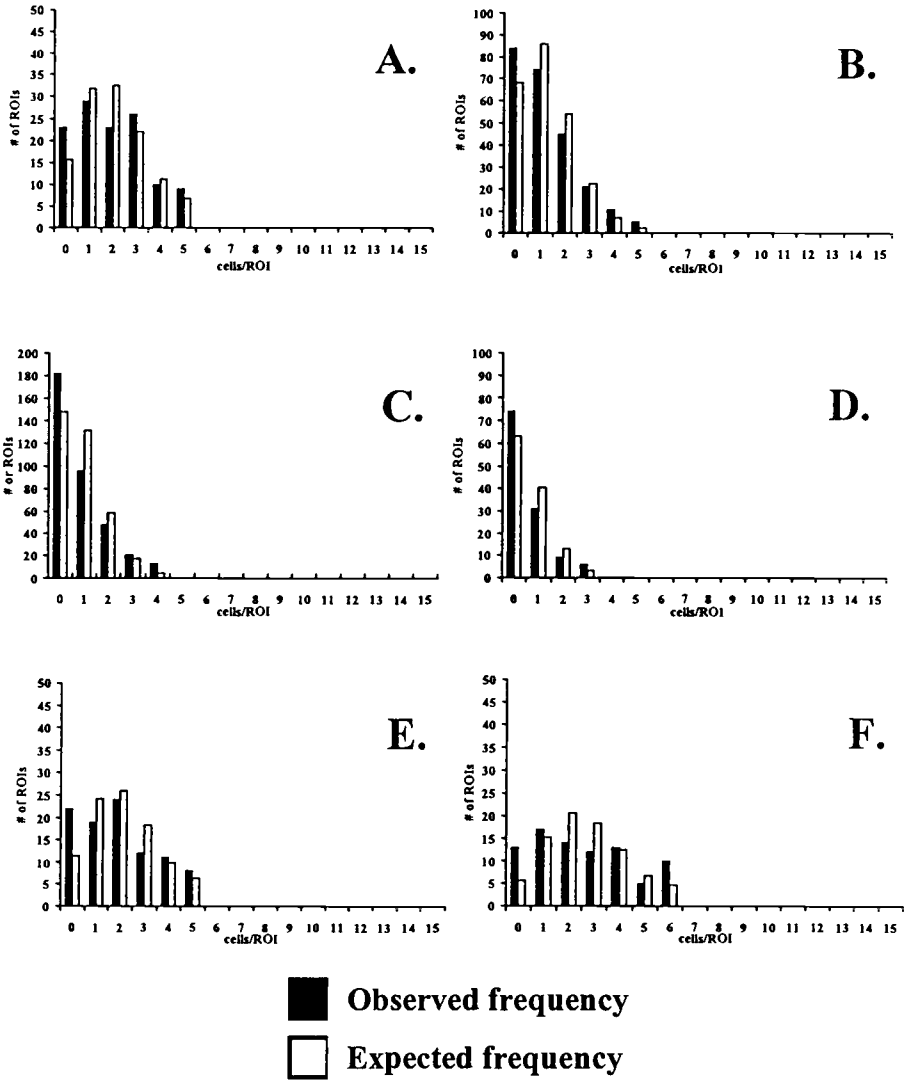

Figure 14. BATS B138 environmental Poisson distributions.

A. Zero meter positive probe microslide. n= 245 μ= 1.26 $\chi^2_{0.05}$= 8.11
B. Zero meter negative control probe microslide. n= 302 μ= 2.04 $\chi^2_{0.05}$= 12.38
C. Twenty-meter positive probe microslide. n= 321 μ= 0.89 $\chi^2_{0.05}$= 34.99 This data set failed the Chi-square Goodness-of-Fit test
D. Twenty-meter negative control probe microslide. n= 277 μ= 0.64 $\chi^2_{0.05}$= 7.56
E. Forty-meter positive probe microslide. n= 205 μ= 2.14 $\chi^2_{0.05}$= 22.36
F. Forty-meter negative control probe microslide. n= 226 μ=2.69 $\chi^2_{0.05}$= 20.37

Oregon Coast environmental cell transfer experiment

Examination of the black PCTE membranes, APES-treated microslides, and standard white PCTE membranes used in this evaluation verified that the transfer protocol resulted in consistently high transfer efficiencies (Table 5). Inspection of the white standard PCTE membranes used in the transfer protocol failed to reveal any cells remaining on the membrane after the cell transfer. Replicate cell counts on three microslides receiving transferred cells average 6.78×10^5 cells per milliliter with a standard deviation (s) of 0.18. Twenty-seven digital image frames were collected and analyzed on each of the three transfer microslides. Frame to frame standard deviations were 5.61, 5.96 and 4.33 for the three microslides, indicating that the cell distribution between and within microslides was comparable. Replicate cell counts on three black PCTE membranes average 6.50×10^5 cells per milliliter with a standard deviation of 0.30. Twenty-seven digital image frames were acquired and analyzed for two of the three replicate cell counts performed on the black PCTE membranes. The third replicate membrane cell count was determined after analysis of twenty-four image frames. Frame to frame standard deviations were 5.47, 8.55 and 7.86 for the three membranes, demonstrating that the cell distribution was consistent between and within membranes. Average cell counts on the microslides and the black PCTE membranes were within four percent of each other, indicating that cells transferred from the standard white PCTE membrane onto the microslide at very high cell transfer efficiency. Estimates of mean cells per

Tube #	Vol. (ml)[a]	Cell counts (x 10^5)			Total objects (n)	White Transfer Membrane (Y/N)[e]
		Black PCTE Membrane[b]	Transfer Slide[c]	CI (L, U)[d]		
1	6.3	6.82	na[f]	(6.28, 7.37)	598	na
2	6.3	na	6.78	(6.23, 7.32)	594	N
3	9.9	6.22	na	(5.80, 6.63)	856	na
4	9.9	6.46	na	(6.01, 6.91)	791	na
5	9.9	na	6.59	(6.16, 7.02)	907	N
6	9.9	na	6.96	(6.52, 7.40)	958	N
		6.50	6.78	**Average of 3 replicates**		
		0.30	0.18	**Standard deviation**		
	104%			**TRANSFER EFFICIENCY**		

Table 5. Cell Counts for the Microslide Transfer Protocol Evaluation.

a. Volume of aged seawater corrected for 10% formalin fixative.
b. Cells filtered onto black PCTE membrane, DAPI stained and directly counted.
c. Cells filtered onto white PCTE membrane, transferred to microslide (transfer slide), PI stained and counted.
d. Confidence Interval based upon Poisson distribution. L= Lower confidence boundary. U= Upper confidence boundary. α= 0.05.
e. Cells filtered onto white PCTE membrane and transferred to microslide (transfer slide). White PCTE membrane was subsequently DAPI stained and examined for residual non-transferred cells. Y = Residual cells observed. N = No residual cells observed.
f. na = not applicable. Cells filtered onto the black PCTE membrane and onto the white PCTE membrane for transfer to the transfer slide are parallel treatments of identical subsamples.

ROI (μ) for the four-eleven milliliter volume samples (9.9 milliliter seawater corrected for 10% formalin fixative) were 2.64, 2.75, 2.8 and 2.96 cells per ROI for

n = 856, 791, 907 and 958 respectively. Average cells per ROI for these four samples was 2.78 (s = 0.13). Estimates of μ for the two-seven milliliter volume samples (6.3 milliliter seawater corrected for 10% formalin fixative) were 1.84 and 1.83 for n = 598 and 594 respectively. Average μ for these two samples was 1.835. The low standard deviations of μ indicated that the distribution of cells within each image frame was consistent. The chi-square (χ^2) Goodness of-Fit test statistic verified that for microslides and black PCTE membranes the number of cells per ROI could be treated as values of a random variable Y having a Poisson distribution at a 0.05 level of significance ($\chi^2_{0.05}$) (Figure 15.). Considering fifteen values of the random variable Y tested the null hypothesis H0 that the cells were distributed in a Poisson manner. One degree of freedom was lost for each parameter obtained from the observed data. The total observed cell frequency for each of the six sets of cell counts data (324, 288, 324, 324, 324, and 324) and the estimate for μ were obtained from the empirical data. The calculated value of $\chi^2_{0.05}$ for thirteen degrees of freedom for each of the six cell distributions (6.86, 9.82, 5.04, 6.17, 15.44 and 2.83) did not exceed the tabulated value of $\chi^2_{0.05} = 22.36$ (Figure 15). The null hypothesis that the cells are distributed in a Poisson manner cannot be rejected for any of the subsamples.

A fundamental objective of the digital analysis of *in situ* hybridization experiments is the categorization of bacterial cells exhibiting positive fluorescence signals when specific oligonucleotide probes are applied. The human eye is capable

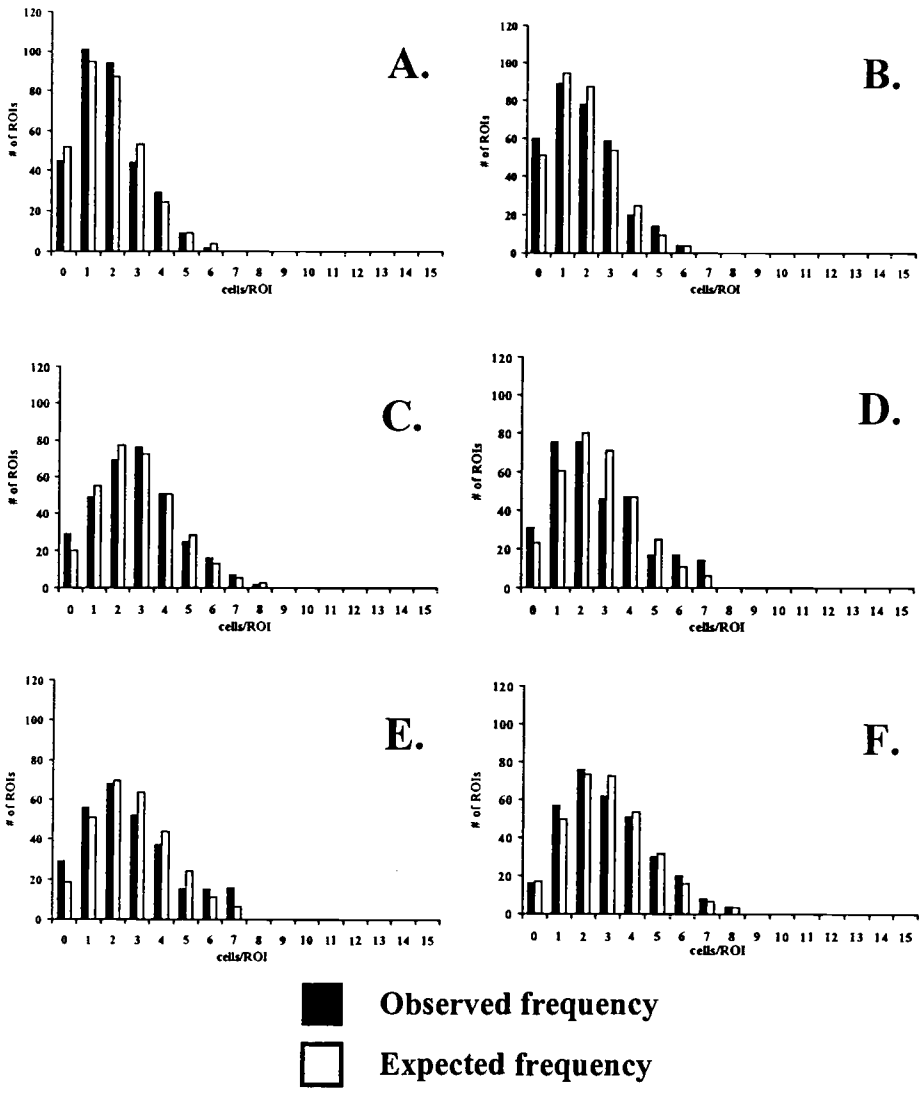

Figure 15: Microslide transfer evaluation Poisson distribution

A. Distribution for seven milliliter sample. Microslide. n=594, μ=1.83. $\chi^2_{0.05}$ = 5.04.
B. Distribution for seven milliliter sample. Black PCTE membrane. n=598, μ=1.84. $\chi^2_{0.05}$ = 6.86
C. Distribution for eleven milliliter sample. Microslide. n=907, μ=2.8. $\chi^2_{0.05}$ = 6.17.
D. Distribution for eleven milliliter sample. Black PCTE membrane. n=856, μ=2.64. $\chi^2_{0.05}$ = 15.44
E. Distribution for eleven milliliter sample. Microslide. n=958, μ=2.96. $\chi^2_{0.05}$ = 2.83.
F. Distribution for eleven milliliter sample. Black PCTE membrane. n=791, μ=2.75. $\chi^2_{0.05}$ = 9.82.

of distinguishing objects based upon multiple criteria simultaneously. In particular the ability of the eye to define object edges under a variety of conditions confers a unique ability to differentiate one type of object from another (16). Automated digital analysis, even with the most sophisticated pattern recognition algorithms, requires that objects of interest possess some intrinsic properties that allow them to be electronically separated from other objects. In the interest of speed and resource requirements, the electronic discrimination should be based upon a minimum of object properties as detected on the digital image frame. The most obvious properties are object intensity and size.

Examination of Table 2 and Figure 10 suggests that cell signals resulting from application of the positive SAR11[4]*Cy3 probe set, negative control probe 338F*Cy3, autofluorescent cells and artifacts can be differentiated from each other based upon signal intensity and object area. However, there was sufficient overlap of these object parameters, evidenced by high standard deviations in the intensity data, to prevent a single rule being applied to facilitate this discrimination.

Limitations in the optical and digital sampling of the fluorescent energy emitted by cells in the sample may be responsible for some of the observed variation. The quality of the digital image acquired for analysis is dependent upon the quality of the optical image projected onto the digital CCD chip. The optical image is formed at the back focal plane of the microscope's objective by collection of light emitted by the cells in the sample (13). In epifluorescence microscopy, the sample plane is flooded with excitation energy of defined bandwidth. For small

objects such as oligotrophic bacterial cells with marginal fluorescence output non-uniform excitation energy may result in an uneven distribution of background grey level values across the digital image frame. The uneven light field may introduce variation in cell signals analyzed in the digital image (data not shown). More importantly, a non-uniform digital background confounds attempts to isolate and electronically mask some objects of interest. Epifluorescence imaging of marine environmental cells requires that the optical components be carefully adjusted to provide an even, slightly diffuse field of illumination

The physiological state of the cells may introduce variation in cell signal intensities. Figure 11 illustrates some of the variation of cell signal within a single field of view. The frequency of probe binding may not be the same for all cells in a sample depending upon ribosome content, differential cell permeability or some other physiological parameter beyond the analyst's control. This factor may be more important when imaging environmental cells and not cells from culture. Cells in culture are more likely to share a common physiological state. Environmental cells, aggregations of several phylogenetic types representing a variety of ecological lifestyles, are less likely to share a common physiological state at any given time.

Many artifacts may be both visually identified and digitally removed from the analysis. Artifacts may be diffuse and hazy, acting to obscure the recognition and delineation of the cells of interest, or may be relatively bright pinpoints with mean areas less than a tenth of a square micron. There are many exceptions and the number and nature of artifacts in an image is dependent upon both the

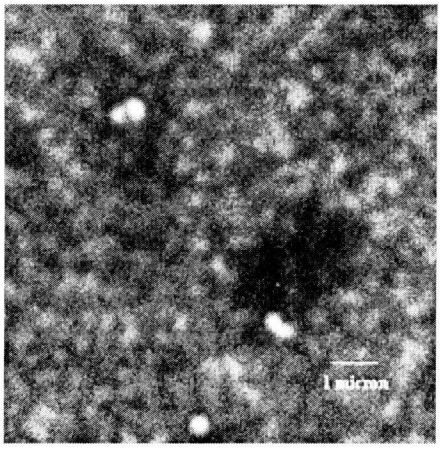

Figure 16. Artifacts presented by poor quality microslide. Debris on the surface prevents delineation and analysis of cells of interest. 650/75-nm bandwidth. 100X objective.

environmental sample and the sample preparation prior to analysis. Poor quality microslides may have sufficient amounts of debris on their surfaces to prevent the analysis altogether (Figure 16). Artifacts observed in the digital image frame as small bright points (Figure 10) could be parsed from the data set by using image analysis software. Artifacts in the BATS BV21 environmental cell data set have a mean area of 0.08 μm^2. This is also the lower limit of the range of areas for objects showing positive fluorescence signals when probed with the SAR11[4]*Cy3 probe set (area range is 0.08 to 0.32 μm^2). Setting a software controlled lower limit of 0.09 μm^2 will effectively prevent the inclusion of this class of artifacts in the analysis. Diffuse artifacts exhibiting low-level fluorescence may be digitally removed from the analysis by application of digital filter processing techniques (Figure 5). However, such techniques are expensive in terms of time and effort, require human intervention and may not be universally effective.

Using a negative control probe such as 338F labeled with the same fluorophore as the positive data probe, as in the B138 cell count analysis can control for autofluorescent cells that appear in the digital image. Cell counts from

the negative control probe slide, which include autofluorescent cells and cells demonstrating non-specific binding, are subtracted from the cell counts obtained using the positive probe. The positive probe counts include positive probe signals, autofluorescent signals and non-specific signals. The net result after subtraction is the cell counts of the positive probe signals only. Autofluorescent cells may confound an analysis further because their large size and bright intensities may wash the weaker probe signal into the image background. Solving this requires digital filtering in the form of grey-level histogram normalization routines, slowing the analysis considerably.

Before protocols using fluorescence signal intensity and object size to automatically differentiate objects of interest from other objects can be considered it is necessary to validate that the fluorescence signals assigned to the objects of interest are credible. This is the issue of probe specificity and the control of stringency conditions in the performance of the *in situ* hybridization experiment. Environmental cell samples are complex in their ecological and phylogenetic diversity, as opposed to samples obtained from culture that exhibit low diversity (monoculture) and controlled environmental conditions. Unless the *in situ* hybridization experiment involves a cultured representative of the environmental sample, it is necessary to determine optimal experimental conditions relying on observations that assume that the cell of interest is being appropriately bound by probe.

The mean area of BATS environmental cells exhibiting positive signals when probed with the SAR11[4]*Cy3 probe set was 0.18 μm^2. The median area for these cells was 0.17 μm^2. The mean area of cells probed with the negative control probe 338F*Cy3 and observed to have putative SAR11 morphology in the DAPI bandwidth was 0.21 μm^2. The median area for these cells was 0.18 μm^2. Therefore, a fraction of the cells observed in the DAPI bandwidth on negative control slides was marginally larger than the expected SAR11 cell size but possess the putative SAR11 morphology. In addition, it was occasionally observed that cells with putative SAR11 morphology on the positive probe slide did not bind SAR11[4]*Cy3 probe (data not shown). The implication was that there are cells in the marine environment that look very much like SAR11 but belong to some other phylogenetic group (comma-shaped *Vibrio* cells, for example).

The lack of a positive control cell for BATS BV21 environmental cell samples is a hindrance to the determination of optimal hybridization and dissociation conditions for *in situ* hybridization experiments, but did not prevent it. Relying upon morphology information gained from microscopic examination and gene sequencing of SAR11 cells in (transient) culture (Connon et al., unpublished data) it is possible to qualitatively assess the specificity of the SAR11[4] probe set with BATS cell samples. Images of the SAR11 cells in (transient) culture revealed a very small (ca. 0.18 μm^2) comma-shaped cell (Figure 17). In environmental samples cells with this comma-shaped morphology and size demonstrated consistently high fluorescence signals when probed with the SAR11[4] probe set. All

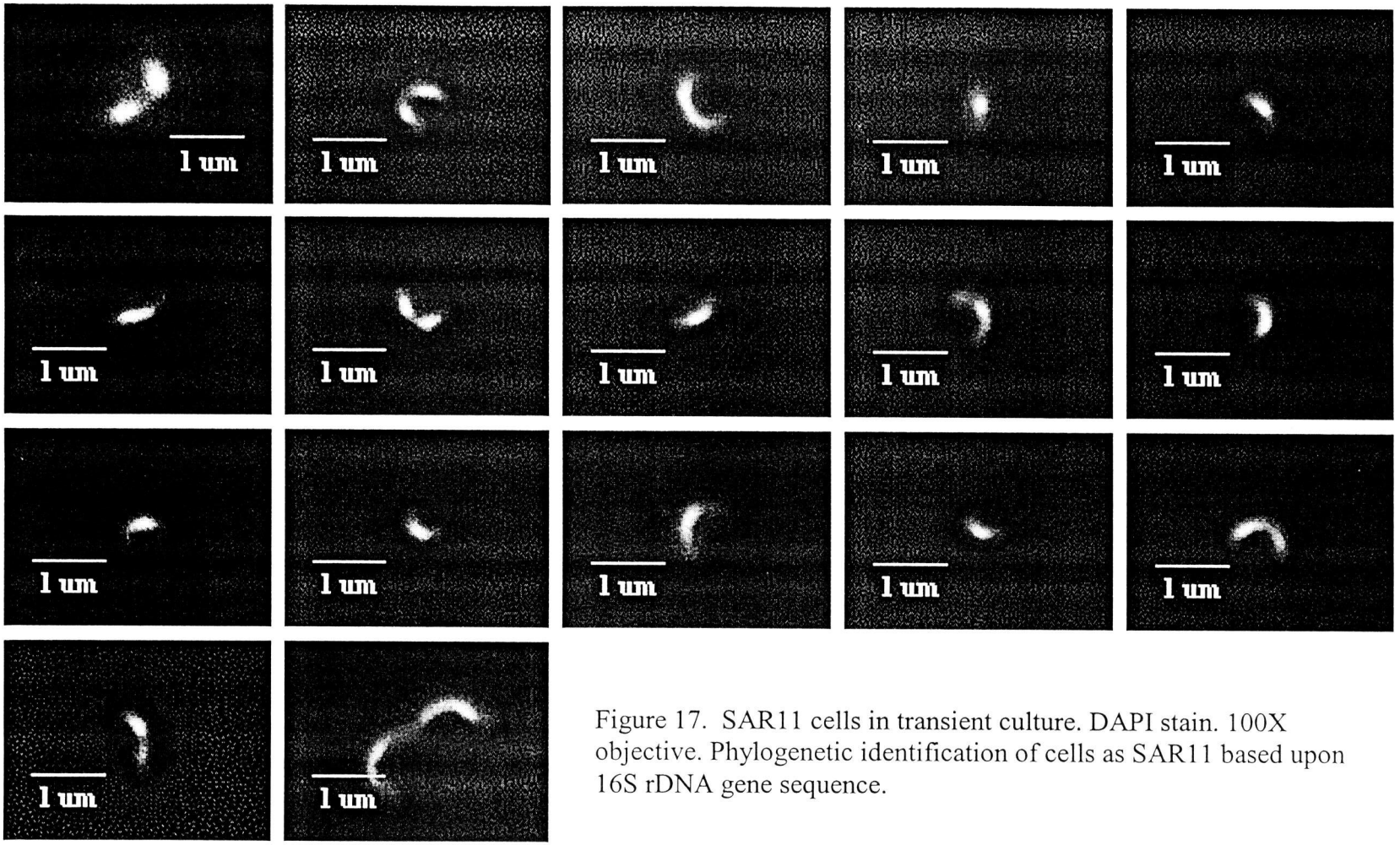

Figure 17. SAR11 cells in transient culture. DAPI stain. 100X objective. Phylogenetic identification of cells as SAR11 based upon 16S rDNA gene sequence.

Probe	Probe Parameters			Stahl & Amann[e.] 1989		Wahl, G.M[f.]. et al. 1987	
	Length (n)	%GC	%formamide	Hyb[a.]	Wash[b.]	Hyb[c.]	Wash[d.]
SAR11-541	18	55.6	35	33.48	39.57	40.48	39.57
SAR11-151	22	43.2	35	36.68	42.77	43.68	42.77
SAR11-440	22	45.5	35	37.62	43.71	44.62	43.71
SAR11-731	23	41.3	35	37.52	43.61	44.52	43.61

Table 6. Theoretical T_m and T_d for SAR11[4] Probe Set (see text for discussion).

a. Hybridization $T_m = 81.5 + 16.6 \log [M] + 0.41 (\%GC) - 820/n - 0.7 (\%formamide)$
b. Wash $T_d = 81.5 + 16.6 \log [M] + 0.41 (\%GC) - 820/n$
c. Hybridization $T_m = 81/5 + 16.6 \log [M] + 0.41 (\%GC) - 820/n - 0.5 (\%formamide)$
d. Wash $T_d = 81.5 + 16.6 \log [M] + 0.41 (\%GC) - 820/n$
e. Stahl & Amann, Development and Application of Nucleic Acid Probes, *in* Nucleic Acid Techniques in Bacterial Systematics,
E. Stackebrandt and M. Goodfellow, ed. 1989.
f. Wahl, Geoffrey M., Shelby L. Berger, and Alan R. Kimmel, Molecular Hybridization of Immobilized Nucleic Acids: Theoretical Concepts and Practical Considerations *in* Methods in Enzymology, Volume 152, Academic Press, Inc. 1987

of the positive probe signals obtained using the SAR11[4]*Cy3 probe set in Table 2 and Figure 10 had the comma-shaped morphology and have a mean area ca. 0.18 μm^2. No other cell morphology has been observed with high positive fluorescence signals when probed with the SAR11[4] probe set. This holds true for the BATS BV21 and B138 environmental samples and all others obtained so far from the Sargasso Sea or Oregon Coast seawater. Due to the low cell concentration and transient nature of the SAR11 culture, rigorous *in situ* hybridization experiments could not be performed with these cultured cells. Therefore, the causative link between the SAR11[4] probe binding the correct complementary target sequence and positive fluorescence signal was not completely established, though the evidence of specific binding of the probe to the appropriate cells in environmental samples is compelling.

Performing hybridizations at 32°C and subsequently washing BATS BV21 environmental cells in low salt buffer (70 mM Na^+) at ca. 3 to 6°C below the theoretical dissociation temperature (T_d) (Table 6) resulted in acceptably high positive cell signals while maintaining probe specificity for the target (Figure 12). Several images acquired at different wash temperatures (all other parameters held constant) of positive SAR11[4]*Cy3 fluorescence signal in the 650/75-nm bandwidth provided evidence for the specificity of the reaction conditions (Figures 18-20). The strategy employed to maximize both probe binding and signal intensity was to hybridize the probe to the cells at permissive equilibrium conditions and subsequently wash both excess and non-specifically bound probe off at high

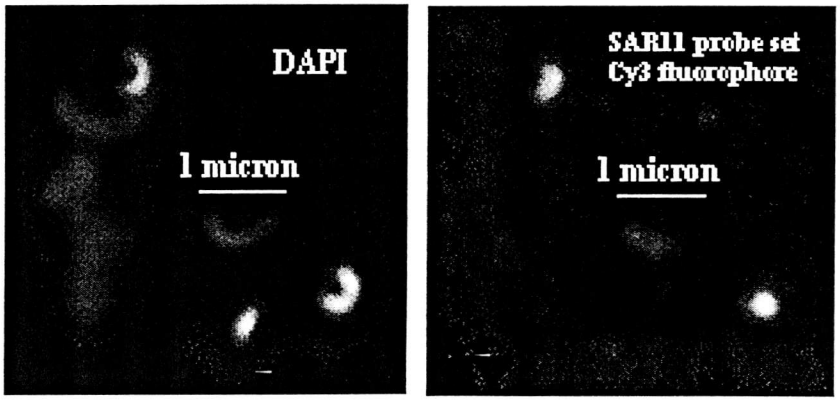

Figure 18. BATS BV21 environmental cells showing specificity to SAR11[4]*Cy3 probe set at 25°C wash. Left: DAPI stained cells. Right: cells probed with SAR11[4]*Cy3 probe set. Hybridizaton at 32°C. 100X objective.

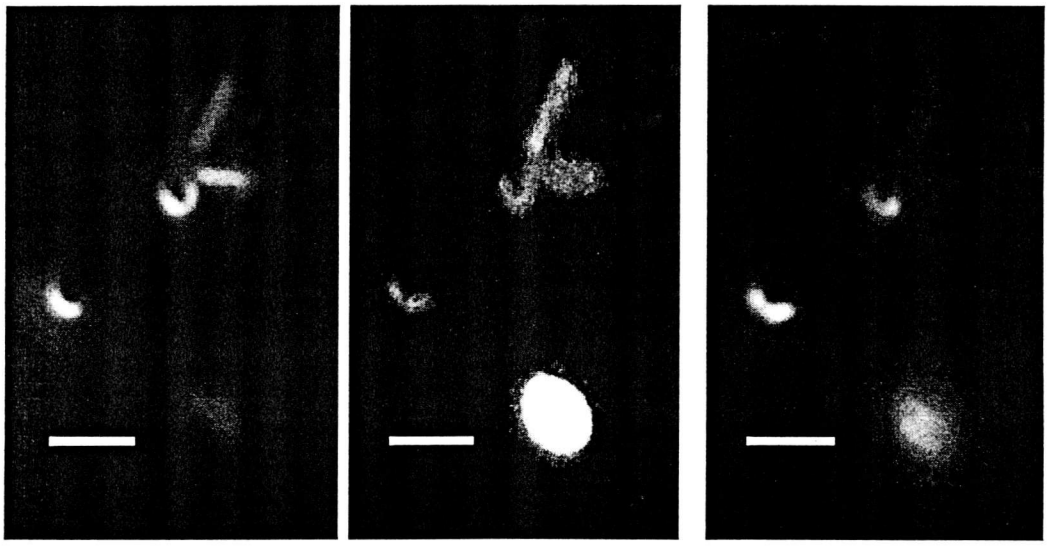

Figure 19. BATS BV21 environmental cells showing specificity to SAR11[4]*Cy3 probe set at 32°C wash.
A. DAPI stained cells
B. Cells probed with bac[3]*FITC probe set
C. Cells probed with SAR11[4]*Cy3 probe set
Hybridization at 32°C. 100X objective. White bar is one micron.

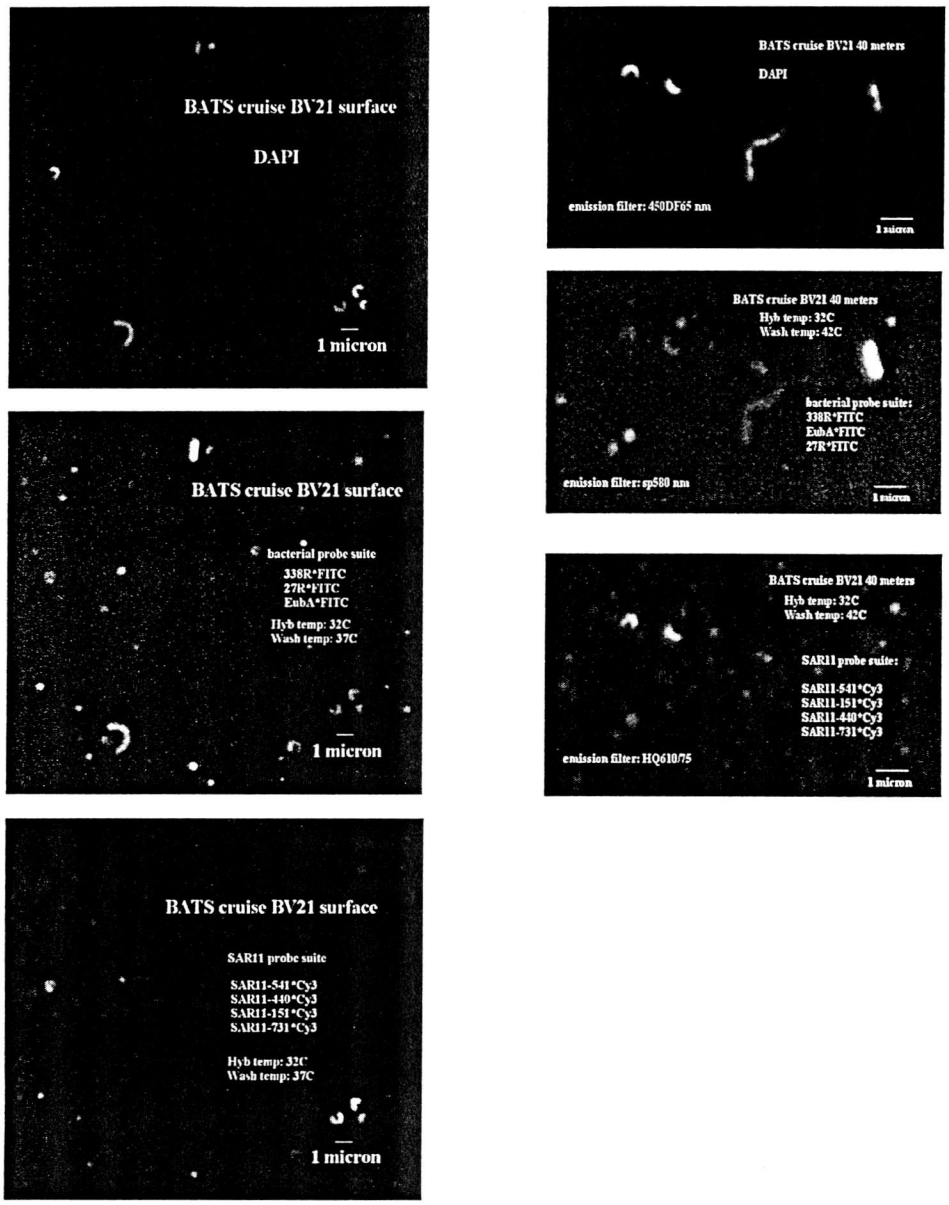

Figure 20. Images of BATS BV21 environmental cells washed at 37C and 42C.

A. DAPI stained cells
B. Cells hybridized with bac[3]*FITC probe set and washed at 37°C
C. Cells hybridized with SAR11[4]*Cy3 probe set and washed at 37°C
D. DAPI stained cells
E. Cells hybridized with bac[3]*FITC probe set and washed at 42°C
F. Cells hybridized with SAR11[4]*Cy3 probe set and washed at 42°C

All hybridizations at 32°C. 100X objective

stringency. The goal was to push the equilibrium toward maximum specific probe binding, even if accompanied by some amount of non-specific binding. Theoretical duplex melting temperatures (T_m) were examined using two equations (Table 6). Each equation differs only in the influence assigned to the concentration formamide, a duplex destabilizing solvent. Wahl et al. 1987 empirically derived an equation that for every 10% increase in formamide concentration the hybridization equilibrium is shifted down 5°C. Using Wahl's equation the four SAR11 probes in the SAR11[4] probe set have calculated values of T_m (35% formamide) of 40.48, 43.68, 44.62 and 44.52°C for SAR11-541, -151, -440 and –731, respectively. Stahl & Amann 1989 modified an equation (Table 6 and Equation 3) designed to calculate T_m for probes longer than fifty nucleotides (18) for use with oligonucleotide probes between ten and fifty nucleotides. This equation attaches greater impact to the formamide concentration than does Wahl's equation. Stahl & Amann's method estimates a drop in T_m of 7°C for every 10% increase in formamide. The calculated T_m (35% formamide) for the four SAR11 probes using Stahl & Amann's equation are 33.48, 36.68, 37.62 and 37.52°C for probe SAR11-541, -151, -440 and –731, respectively. Hybridization of BATS BV21 and B138 environmental cells at 32°C represents permissive conditions according to both equations. Since the hybridization step of the reaction is an equilibrium that depends upon the first order kinetics of probe to target collisions it is desirable to perform the hybridization step at slightly elevated temperatures to facilitate reaction rates.

The wash step of the reaction is designed to remove excess and non-specifically bound probe from the reaction system. Theoretical temperatures of dissociation are estimated using a single equation (Table 5 and Equation 3) the most important variable of which is the concentration of the monovalent cation ($[Na^+]$). At a low salt concentration of 70 mM Na^+ the estimated T_d for the four SAR11 probes is 39.57, 42.77, 43.71 and 43.61°C for probe SAR11-541, -151, -440 and –731, respectively. Figure 12.indicates that a wash temperature of 37°C leaves enough specifically bound probe to emit relatively high signal intensity per cell (65.28 grey levels above background) while removing excess and non-specifically bound probe (Figure 20).

Once the objects of interest have been differentiated from other objects in the digital image frame by visual or digital criteria and it is certain (or very likely) that the positive signals observed in the images are linked to the cells of interest by a specific probe reaction the most common analytical objective is to count the objects.

The Sargasso Sea BATS BV21 environmental samples are valuable for classifying objects and establishing hybridization reaction parameters but are unsuitable for cell counting experiments. The cell retention rate of 1 to 8% post-concentration protocol is insufficient for the analytical determination of cell counts and the determination of the fraction of SAR11[4] positive cells in the original environmental sample. Potential phylogenetic bias associated with such low retention rates relative to the natural system is unproven but possible. Phylogenetic

bias may be introduced because of the physical properties of a particular cell type (sticky cell wall, for example) or size.

Large cells, with greater surface area in contact with the membrane used in the concentration protocol may stick preferentially to the membrane. Small cells may be lost in the centrifugation step of that protocol. Any physical feature of a cell type influencing its behavior in the concentration protocol threatens to skew the relative fractions of phylogenetic groups remaining.

Digital images of BV21 sample preparations reveal significant clumping of the cells. Ideal cell counts require a consistent distribution of cells across the surface of the microslide or membrane. The average cells detected per image frame should be consistent for all of the slides included in the analysis if each slide represents an identical subsample. Standard deviations between digital image frames on a given slide should be low and comparable.

The frame-to-frame cell count averages for BATS B138 environmental cell samples vary widely from 7.5 cells per frame for the twenty-meter negative control slide to 32.3 cells per frame for the forty-meter negative control slide. The frame-to-frame standard deviation on the twenty-meter negative control slide is 4.91, indicating that each image frame included in the analysis varied significantly in the number of cells counted. Examination of the average cells per frame and frame-to-frame standard deviations for the B138 slide preparations indicated that the cells are inconsistently distributed across the surface of each microslide. Calculating the chi-square test statistic for the cell distribution on each slide reveals the degree of

deviation from true Poisson distribution (Figure 14). Two of the distributions, the zero-meter positive probe slide and the twenty-meter negative control probe slide have low values of the calculated Chi-square test statistic, presenting reasonable evidence that they are distributed in a Poisson manner. However, the low average cell counts per image frame and high frame-to-frame standard deviation for the twenty-meter negative control probe slide diminishes the statistical credibility of this sample. The least reliable sample in the data set is the twenty-meter positive probe slide, which fails to meet the standards of fit to a Poisson distribution, displays low average cell counts per frame and a high frame-to-frame standard deviation. The most reliable sample in the data set is the zero-meter positive probe slide, showing a high average number of cells counted per image frame, a low frame-to-frame standard deviation and a low chi-square test statistic relative to the ideal Poisson distribution. These are the fundamental parameters that define the quality of a cell distribution for counting.

The cause of the poor cell distributions is likely linked to the transfer protocol used to transfer cells filtered onto PCTE membranes onto microslides. This conclusion is supported by the large variation in the average number of cells detected per image frame for each of the sample slides. Without comparative distribution data from the membranes used to generate the BATS direct counts it is not possible to determine that the transfer protocol *per sae* resulted in the marginal cell distributions observed in this data set. It is possible that the distribution of cells on the membranes were flawed prior to transfer.

A biological system that undergoes a rigorous statistical or mathematical analysis must also be evaluated in terms of the biological sense of the results. The objective of the BATS B138 environmental cell sample analysis is to calculate the percentage of SAR11 cells in the water column. Assuming that specificity criteria for the SAR11[4] probe set are met the analysis indicates that at zero meters in March 2000 11.79% of all cells accepting DAPI nuclear stain were SAR11. Acknowledging that less than ideal cell distribution and counting statistics for the twenty-meter samples limit the utility of the data the calculated abundance of SAR11 cells relative to DAPI stained cells in the water column at this depth is 23.81%. At forty-meter depth in March 2000 SAR11 cell abundance is 33.14% of the DAPI stained cells according to these counts. Previous experiments applying radioactively labeled [^{32}P] oligonucleotide probes to environmental genomic DNA immobilized on membrane indicate that SAR11 gene clone abundance is ca. 25 to 27% (9). Even with the limited applicability of the twenty-meter data set it appears that the *in situ* probing of the water column provides values comparable to established quantitative methods.

Cell counting using traditional image analysis techniques requires that the density and distribution of a relatively small sample of cells be representative of the total population of cells on the microslide or membrane. On average, ca. 0.005% of the cells on the microslide or membrane will be counted using the 100X objective. Approximately 0.005% of the surface area of the membrane or microslide will be imaged. From this data statistically relevant cell counts are to be obtained and

applied to the natural system from which the cells were collected. For that to be possible, the entire density and distribution of cells on the membrane or microslide must fit a Poisson distribution. Cells that are drawn onto porous membrane under gentle vacuum filtration are likely, under most circumstances, to be Poisson distributed. Cells on membranes that are subjected to transfer to microslides using a transfer protocol may not be distributed in a Poisson manner if the transfer efficiency is low. Low transfer efficiency often results in patchiness in the cell mass on the microslide. Careless handling of the membrane during the transfer such as dragging the membrane across the microslide surface may skew the resulting distribution of transferred cells. The distribution of cells on either membrane or microslide may be negatively impacted by cell clumping. Moreover, in order that fluorescent signals resulting from the application of oligonucleotide probes to the cells be detected and analyzed, those signals must stand out from the background sufficiently to permit delineation of cell shapes. Two approaches, used simultaneously, accomplish this. The first involves the application of multiple probe sets, such as the SAR11[4] set, to the cells to boost each individual cell's fluorescence signal. The second involves lowering the background grey level values of the supporting substrate to improve contrast and facilitate cell border delineation.

The second approach, lowering the background grey level values, is addressed by transferring cells collected on membranes to treated microslides. The mean background grey level intensity of the microslide relative to the membrane is much lower. The BATS B138 environmental cell analysis suggested that

improvements had to be made in the cell transfer protocol used to mount cells on microslides. The original cell transfer protocol provided a quick method of transferring cells previously drawn onto a PCTE membrane over to a glass microslide. The protocol was introduced due to the inherent signal/noise problem encountered when performing in situ hybridization experiments with environmental cells samples on membranes. The transfer protocol reduces background fluorescence levels as well as relieving the negative impact of focal irregularities arising from minute folds and general unevenness of the membrane.

A modified transfer protocol was developed to address these problems as well as provide acceptable cell distributions for counting analysis. The influence of each parameter of the modified transfer protocol on the increase in cell transfer efficiency has not been experimentally determined. Two changes are probably most beneficial.

A protocol was developed to pre-treat ultraclean microslides with 3-aminopropyltriethoxysilane (APES), a solvent that reacts with hydroxyl groups in glass substrates, enabling amino-alkyl groups on the cell surface to bind covalently to the microslide. This treatment proves superior to the manufactured SuperFrost Plus microslides used in the BATS B138 cell sample preparations with respect to enhanced cell transfer efficiency. The APES-treated microslides are simply 'stickier.'

During the transfer procedure, a four-inch rubber brayer is used to firmly press the cells on the transfer membrane onto the microslide, insuring that all of the

cells on the membrane come into contact with the microslide prior to incubation. Membranes were applied to the microslides immediately after the cells were filtered onto them without allowing them to dry out.

The modified transfer protocol resulted in very high transfer efficiency for three replicate cell transfers. The resulting cell distributions closely fit an ideal Poisson distribution. However, despite initial success integrating the method into the *in situ* hybridization protocol, an apparent cross-reaction between oligonucleotide probe and the APES-treated microslide quickly became apparent, confounding subsequent experiments. The nature and cause of the cross-reaction remains unknown. However, the modified transfer protocol works acceptably well on manufactured pre-treated SuperFrost Plus microslides. Transfer efficiencies greater than 90% onto SuperFrost Plus microslides have been observed (data not shown). The use of SuperFrost Plus microslides presents a different set of problems, as many lots of these microslides are debris-laden (Figure 16) and unacceptable for analysis.

CONCLUSIONS

Summary

The objectives of this work were to develop digital imaging protocols specifically applicable to the study of marine bacterial cells using Fluorescence *in situ* Hybridization techniques, and to test these protocols on marine environmental cells from the Bermuda Atlantic Time Series Station in the Sargasso Sea.

The data shows that the positive probe signals observed when environmental cell samples from BATS are hybridized with the SAR11^{4}*Cy3 probe set are ubiquitously associated with bacterial cells having a comma-shaped morphology, and that those bacterial cells are members of the SAR11 phylogenetic group.

The fraction of SAR11 cells obtained from BATS in March 2000 is consistent with previous clone library data (25% of the total cells).

Future Work

The next generation of digital chip technology may provide the sampling resolution required to automate image analytical processing of marine environmental cells. Continued work on improving the depth-of-field and focal irregularities is required.

The use of "helper" probes to facilitate the binding of fluorescently labeled probes is recommended. The issue of signal to noise ratio and probe binding must continue to be addressed.

BIBLIOGRAPHY

1. Amann, R.I., L. Krumholz, D.A. Stahl 1990. Fluorescent-oligonucleotide probing of whole cells for determinative, phylogenetic, and environmental studies in microbiology J. Bacteriol. 172: 762-770

2. Azam, F., T. Fenchel, J.G. Field, J.S. Gray, L.A. Meyer-Reil, and F. Thingstad 1983. The ecological role of water-column microbes in the sea Mar. Ecol. Prog. Ser. 10:257-263

3. Chisholm, S.W., R.J. Olson, E.R.Zettler, J. Waterbury, R. Goericke, and N. Welschmeyer 1988. A novel free-living prochlorophyte abundant in the oceanic euphotic zone Nature (London) 334: 340-343

4. Daft, M.J., and W.D. Stewart 1973. Light and electron microscope observations on algal lysis by bacterium CP-1 New Phytology 72: 366-375

5. Field, K.G., D. Gordon, T.D. Wright, M.S. Rappe, E. Urbach, K.L.Vergin, and S. Giovannoni 1997. Diversity and depth-specific distribution of SAR11 cluster of rRNA genes from marine planktonic bacteria Appl. Envir. Microbiol. 63: 63-70

6. Fogg, G.E. 1966. The extracellular products of algae Oceanogr. Mar. Biol. Annu. Rev. 4:195-212

7. Fuhrman, J.A., and F. Azam 1980. Bacterioplankton secondary production estimates for coastal waters of British Columbia, Antarctica, and California Appl. Environ. Microbiol. 39: 1085-1095

8. Fuhrman, J.A., and F. Azam 1982. Thymidine incorporation as a measure of heterotrophic bacterioplankton production in marine surface waters: evaluation and field results Mar. Biol. 66: 109-120

9. Giovannoni, S.J., and M.S. Rappe 2000. Evolution, Diversity, and Molecular Ecology of Marine Prokaryotes *in* D.L. Kirchman (ed.), Microbial Ecology of the Oceans Wiley-Liss, Inc.

10. Glockner, F.O., R.I. Amman, A. Alfreider, J. Pernthaler, R. Psenner, K. Trebesius, and K.H. Schleifer 1996. An In-Situ Hybridization Protocol for Detection and Identification of Planktonic Bacteria System. Appl. Microbiol. 19:403-406

BIBLIOGRAPHY (Continued)

11. Golterman, H.L. 1964. Mineralization of algae under sterile conditions or by bacterial breakdown Int. Ver. Theor. Angew. Limnol. Verh. 15: 544-548

12. Gunnison, D., and M. Alexander 1975. Resistance and susceptibility of algae to decomposition by natural microbial communities Limnol. Oceanogr. 20

13. Inoue, S., and K.R. Spring 1997. Video Microscopy: The Fundamentals, Second Edition. Plenum Press, New York.

14. Kirchman, D., J. Sigda, R. Kapuscinski, and R. Mitchell 1982. Statistical Analysis of the Direct Count Method for Enumerating Bacteria Appl. Envir. Microbiol. 44:376-382

15. Mankaeva, K.A. 1966. Studies of lysis in cultures of *Chlorella* Microbiology 35: 2303-2310

16. Marr, D., and E. Hildreth 1980. Theory of Edge Detection Proc. R. Soc. Lond. B. 207: 187-217

17. McConaughy, B.L., C.D.Laird, and B.J.McCarthy 1969. Nucleic Acid Reassociation in Formamide Biochemistry 8: 3289-3295

18. Meinkoth, J., and G. Wahl 1984. Hybridization of nucleic acids immobilized on solid supports Anal. Biochem. 138: 267-284

19. Ott, R.I. 1993. An Introduction to Statistical Methods and Data Analysis. Wadsworth Publishing Co., Belmont, California

20. Ramsing, N.B., H. Fossing, T.G. Ferdelman, F. Anderson, and B. Thamdrup 1996. Distribution of Bacterial Populations in a Stratified Fjord (Mariager Fjord, Denmark) Quantified by In Situ Hybridization and Related to Chemical Gradients in the Water Column Appl. Envir. Microbiol. 64: 294-303

21. Rappe, M.S., P.F. Kemp, and S. Giovannoni 1997. Phylogenetic Diversity of Marine Coastal Picoplankton 16S rRNA Genes Cloned from the Continental Shelf off Cape Hatteras, North Carolina Limnol. Oceanogr. 42: 811-826

BIBLIOGRAPHY (Continued)

22. Rappe, M.S., M.T. Suzuki, K.L. Vergin, and S.J. Giovannoni 1998. Phylogenetic Diversity of Ultraplankton Plastid Small-Subunit rRNA Genes Recovered in Environmental Nucleic Acid Samples from the Pacific and Atlantic Coasts of the United States Appl. Envir. Microbiol. 64: 294-303

23. Stahl, D.A., and R. Amann 1989. Development and Application of Nucleic Acid Probes, p. 205-248. In E. Stackebrandt, and M. Goodfellow (eds.), Nucleic Acid Techniques in Bacterial Systematics.

24. Staley, J.T., and A. Konopka 1985. Measurement of in situ activities of nonphotosynthetic microorganisms in aquatic and terrestrial habitats Annu. Rev. Microbiol. 39: 321-346

25. Stockner, J.G., and N.J.Antia 1986. Algal picoplankton from marine and freshwater ecosystems: a multidisciplinary perspective Can. J. Fish. Aquat. Sci. 43: 2472-2503

26. Wahl, G.M., S.L. Berger, and A.R. Kimmel 1987. Molecular Hybridization of Immobilized Nucleic Acids: Theoretical Concepts and Practical Considerations, p. 399-407, Methods in Enzymology, vol. 152 Academic Press.

27. Waterbury, J.B., S.W.Watson, R.L.Guillard, and L.E. Brand 1979. Widespread occurrence of a unicellular, marine, planktonic cyanobacterium Nature (London) 227: 293-294

28. Weiss, S.B., W.T. Hsu, J.W. Foft, and N.E. Scherberg 1968. Proc. Natl. Acad. Sci. USA 61: 114

29. Wright, T.D., K.L.Vergin, P.W. Boyd, and S.J. Giovannoni 1997. A Novel α-Subdivision Proteobacterial Lineage from the Lower Ocean Surface Layer Appl. Envir. Microbiol. 63: 1441-1448